A genome-wide CRISPR/Cas9 knock-out screen identifies the DEAD box RNA helicase DDX42 as a broad antiviral inhibitor

Boris Bonaventure[1], Antoine Rebendenne[1*], Francisco Garcia de Gracia[1*], Joe McKellar[1*], Ségolène Gracias[2], Emmanuel Labaronne[3], Marine Tauziet[1], Ana Luiza Chaves Valadão[1], Eric Bernard[1], Laurence Briant[1], Nathalie Gros[4], Wassila Djilli[1], Mary Arnaud-Arnould[1], Valérie Courgnaud[5], Hugues Parrinello[6], Stéphanie Rialle[6], Reiner Schulz[7], Emiliano Ricci[3], Nolwenn Jouvenet[2], Olivier Moncorgé[1] and Caroline Goujon[1#]

1 IRIM, CNRS, Université de Montpellier, France

2 Institut Pasteur, Virus Sensing and Signaling Unit, Department of Virology, CNRS UMR 3569, Paris, France

3 LBMC, Université de Lyon, ENS de Lyon, CNRS, INSERM, Lyon, France

4 CEMIPAI, CNRS, Université de Montpellier, France

5 IGMM, CNRS, Université de Montpellier, France

6 Montpellier GenomiX (MGX), Biocampus, CNRS, INSERM, Université de Montpellier, France

7 Department of Medical & Molecular Genetics, King's College London, United Kingdom

* Contributed equally to the work

[#] Corresponding and lead author: Caroline Goujon, IRIM UMR9004, 1919 route de Mende, 34293 Montpellier cedex 5. Phone: +33 4 34 35 94 33, e-mail: caroline.goujon@irim.cnrs.fr, ORCID iD: 0000-0001-8571-1108

Abstract

Genome-wide CRISPR/Cas9 knock-out genetic screens are powerful approaches to unravel new regulators of viral infections. Here, we took advantage of the ability of interferon (IFN) to restrict HIV-1 infection, in order to create an environment hostile to replication and reveal new inhibitors through a CRISPR screen. This approach led to the identification of the RNA helicase DDX42 as an intrinsic inhibitor of HIV-1. Depletion of endogenous DDX42 increased HIV-1 DNA accumulation and infection in several human cell lines and primary cells, irrespectively of IFN treatment. DDX42 overexpression inhibited HIV-1, whereas a dominant-negative mutant of DDX42 increased infection. Importantly, DDX42 restricted retrotransposition of long interspersed elements-1 (LINE-1), infection with other retroviruses and positive-strand RNA viruses, including Chikungunya virus (CHIKV) and severe acute respiratory syndrome coronavirus 2 (SARS-CoV-2). However, DDX42 did not inhibit infection with negative-strand RNA viruses such as influenza A virus (IAV), arguing against a general, unspecific effect on target cells. In line with this, RNA-seq analysis did not reveal changes upon DDX42 depletion that could explain the observed phenotypes. Proximity ligation assays showed that DDX42 was found in the vicinity of viral elements during infection, and RNA immunoprecipitation confirmed DDX42 interaction with RNAs from LINE-1, CHIKV and SARS-CoV-2, but not IAV. This strongly suggested a direct mode of action of DDX42 on viral ribonucleoprotein complexes. Taken together, our results identify DDX42 as a new, broadly active intrinsic antiviral inhibitor.

46 **Introduction**

47 The intrinsic and innate immunity are at the frontline against viral invasion and provide a rapid
48 and global defence. The innate immunity relies on viral sensing by Pathogen Recognition
49 Receptors (PRRs) inducing the production of type 1 and 3 interferons (IFNs). Secreted IFNs bind
50 to specific receptors and activate the JAK-STAT signalling cascade, which leads to the expression
51 of hundreds of IFN-stimulated genes (ISGs). The cellular reprogramming induced by ISG
52 expression allows the establishment of an antiviral state that efficiently limits viral replication.
53 Some ISGs are indeed direct antiviral effectors harbouring powerful antiviral activities[1]. In addition
54 to the IFN response, antiviral proteins that are constitutively expressed are able to immediately
55 counteract incoming virus replication and are referred to as intrinsic inhibitors; they are part of the
56 so-called intrinsic immunity.

57 Intensive efforts have been made over the past decades to identify genes able to limit viral
58 replication. Several ISGs were identified a long time ago as major players of innate immunity
59 against viruses, such as the myxovirus resistance protein 1 (MX1) Dynamin Like GTPase,
60 2′,5′-oligoadenylate synthetases (OASs) and ribonuclease L (RNASeL), or protein kinase R
61 (PKR)[2–4]. More recently, gain-of-function and loss-of-function screens have identified new IFN-
62 induced antiviral effectors[5–7]. A growing list of cellular proteins with various functions has hence
63 been identified as capable of limiting different steps of virus life cycles[8–10]. Viruses have often
64 evolved to counteract the action of these so-called restriction factors. However, type 1 IFNs (e.g.
65 IFN-alpha and -beta) induce, through the expression of ISGs, an antiviral state particularly
66 efficient at inhibiting HIV-1 when cells are pre-exposed to IFN[9]. The dynamin-like GTPase MX2,
67 and, recently, the restriction factor TRIM5α, have both been shown to participate in this IFN-
68 induced inhibition[6,11–13]. While numerous antiviral ISGs have been identified, less is probably
69 known about the extent of the intrinsic, antiviral inhibitor repertoire. The recent identification of
70 TRIM7 as an enterovirus inhibitor illustrates the fact that important intrinsic, antiviral inhibitors
71 most certainly remain to be revealed[14].

72 With the hypothesis that additional HIV-1 inhibitors remained to be identified, we took advantage
73 of the hostile environment induced by IFN to develop a whole-genome, CRISPR/Cas9 screen

74 strategy in order to reveal intrinsic and innate inhibitors. This strategy led us to identify DDX42 as
75 a new intrinsic inhibitor of HIV-1. We reveal that endogenous DDX42 is antiviral in various cell
76 types, including primary targets of HIV-1, and impairs the accumulation of viral DNA. Moreover,
77 our data show a broad activity against lentiviruses and the retrovirus Murine Leukemia Virus
78 (MLV). Reminiscent of other HIV-1 inhibitors such as APOBEC3G, DDX42 also blocks LINE-1
79 spread by interacting with their RNAs. Interestingly, while three different negative strand RNA
80 viruses were found insensitive to DDX42, several positive strand RNA viruses, including the
81 flavivirus Zika (ZIKV), the alphavirus Chikungunya (CHIKV) and the severe acute respiratory
82 syndrome coronavirus 2 (SARS-CoV-2), were inhibited by this non-processive RNA helicase.
83 Finally, RNA immunoprecipitation assays showed that DDX42 specifically binds to viral RNAs
84 from sensitive viruses, suggesting a direct mode of action. Overall, our study sheds light on a new
85 intrinsic, antiviral function of a so far poorly studied DEAD-box RNA helicase, and provide new
86 insights on a broad-spectrum antiviral inhibitor.
87
88 **Results**
89 The Genome-Scale CRISPR Knock-Out (GeCKO) sgRNA library[15–17] was used to generate
90 knock-out (KO) populations in the glioblastoma T98G cell line. This cell line is both highly
91 permissive to HIV-1 infection and potently able to suppress infection following type 1 IFN
92 treatment (Fig. S1A). The screen strategy is depicted in Figure 1A. Cas9-expressing T98G cells
93 were independently transduced with lentiviral vectors (LVs) coding the two-halves of the GeCKO
94 library, at a low multiplicity of infection (MOI). Next-generation sequencing showed more than
95 94% sgRNA coverage for each sub-library (not shown). Cells were pre-treated with type 1 IFN
96 (IFN-alpha) and incubated with VSV-G-pseudotyped, HIV-1 based LVs coding for an antibiotic
97 resistance cassette. The cells which were successfully infected despite the IFN treatment were
98 selected by survival in the presence of antibiotics. In order to enrich the populations with mutants
99 of interest and to limit the presence of false-positives, two additional rounds of IFN treatment,
100 infection and selection (with different antibiotics) were performed. As expected, the cells enriched
101 after each round became less refractory to HIV-1 infection following IFN treatment (Fig. S1B).

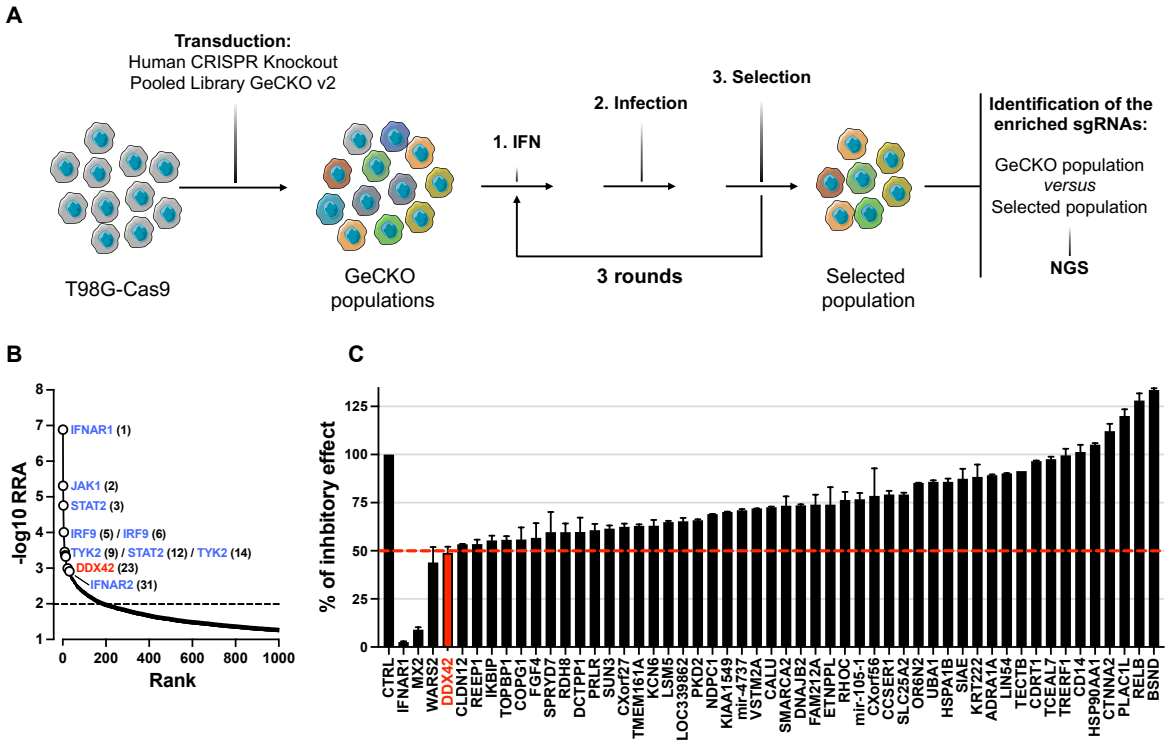

Figure 1. A whole-genome CRISPR/Cas9 screen to identify new HIV-1 inhibitors.

A. Screen strategy. GeCKO cell populations (obtained by transduction of T98G/Cas9 cells with GeCKO v2 LV library) were IFN-treated, challenged with HIV-1 LVs coding for an antibiotic resistance gene and selected. Three rounds of IFN treatment, infection and selection were performed. Genomic DNAs of initial GeCKO and 3-time selected populations were extracted, the sgRNA-coding sequences amplified and sequenced.

B. Candidate gene identification. MAGeCK computational statistical tool[18] was used to establish a Robust Rank Aggregation (RRA) score for each gene based on sgRNA enrichment and number of sgRNAs per gene. Genes belonging to type 1 IFN response pathway (in blue) and DDX42 (in red) are shown (respective ranks into brackets) for 2 independent screens (the results of which were merged in the analysis).

C. Candidate validation. T98G/Cas9/CD4/CXCR4/Firefly KO populations were generated for the 25 top hits of each screen. The control (CTRL) condition represents the mean of 4 negative CTRL populations, obtained with 4 non-targeting sgRNAs; *IFNAR1* and *MX2* KO populations were used as positive controls. KO cell populations were treated with IFN and infected with HIV-1 Renilla and luciferase signals were measured 24 h later (Renilla signals were normalized to Firefly). IFN inhibition (i.e. ratio of untreated / IFN-treated conditions) was calculated and set at 100% inhibition for CTRL. A representative experiment is shown (mean and standard deviation from technical duplicates).

The differential sgRNA abundance between the initial GeCKO populations and selected populations was analysed by next-generation sequencing (NGS) and the MAGeCK algorithm was used to rank the gene candidates (Fig. 1B). An enrichment was observed for 200 genes (RRA score > 0,01), with the best hits being *IFNAR1*, *JAK1* and *STAT2* (Fig. 1B). The crucial mediators of type 1 IFN signalling cascade were among the top hits in both screens (with the notable

125 exception of *STAT1*), validating our approach and confirming the identification of relevant genes.
126 Interestingly, most of the other candidates displayed unknown functions, or functions that were *a*
127 *priori* unrelated to innate immunity. Of note, very little overlap was observed between the two
128 independent screens, performed with two sub-libraries. However, such a poor overlap between
129 biological replicates has been observed before and does not preclude obtaining valid data[19]. The
130 top 25 candidate genes from each screen were selected for further validation. T98G/Cas9 cells
131 expressing HIV-1 CD4 and CXCR4 receptors, as well as Firefly luciferase as an internal control
132 (T98G/Cas9/CD4/CXCR4/Firefly cells), were transduced with sgRNA-expressing LVs to generate
133 individual KO populations, using the identified sgRNA sequences. Four irrelevant, non-targeting
134 sgRNAs, as well as sgRNAs targeting *IFNAR1* and *MX2*, were used to generate negative and
135 positive control populations, respectively. The KO cell populations were pre-treated with IFN and
136 infected with an HIV-1 reporter virus expressing Renilla luciferase and bearing HIV-1 envelope[20]
137 (hereafter called HIV-1 Renilla). Infection efficiency was analysed 30 h later (Fig. 1C). As
138 expected[11,21,22], *IFNAR1* and *MX2* KO fully and partially rescued HIV-1 infection from the
139 protective effect of IFN, respectively. The KO of two candidate genes, namely *WARS2* and
140 *DDX42*, allowed a partial rescue of HIV-1 infection from the IFN-induced inhibition, suggesting a
141 potential role of these candidate genes in HIV-1 inhibition.
142
143 DDX42 is a member of the DEAD box family of RNA helicases, with RNA chaperone activities[23]
144 and, as such, retained our attention. Indeed, DEAD box helicases are well-known to regulate HIV-
145 1 life cycle[24]. However, to our knowledge, the impact of DDX42 on HIV-1 replication had never
146 been studied. In order to validate the effect of *DDX42* KO on HIV-1 infection in another model cell
147 line, two additional sgRNAs were designed (sgRNA-2 and -3) and used in parallel to the one
148 identified in the GeCKO screen (sgDDX42-1) (Fig. 2A). U87-MG/CD4/CXCR4 cells were used
149 here, as we previously extensively characterized the IFN phenotype in these cells[11]. Control and
150 *DDX42* KO cell populations were generated. Control and DDX42 KO cell populations were pre-
151 treated or not with IFN prior to infection with HIV-1 Renilla. Of note, CRISPR/Cas9 KO of *DDX42*
152 induced only a partial decrease of DDX42 protein levels (Fig. 2A) and cell populations derived

153 quite rapidly (not shown), suggesting an essential role for DDX42 in cell survival or proliferation.
154 We observed however that DDX42 partial depletion with all 3 sgRNAs improved HIV-1 infection,
155 confirming that endogenous DDX42 had a negative impact on HIV-1 replication. Interestingly, the
156 increase in infection efficiency induced by *DDX42* KO was observed independently of the IFN
157 treatment. DDX42 is not an ISG, as shown in several cell lines (e.g. U87-MG, T98G, HEK293T)
158 and in primary T cells and monocyte-derived macrophages (Fig. S2A and GSE46599[11]). The fact
159 that the IFN-induced state is at least partially saturable (Fig. S1A) explains why an intrinsic
160 inhibitor of HIV-1, which is not regulated by IFN, could be identified by our approach. Indeed,
161 removing one barrier to infection presumably rendered the cells more permissive and, in this
162 context, IFN had less of an impact on viral replication.

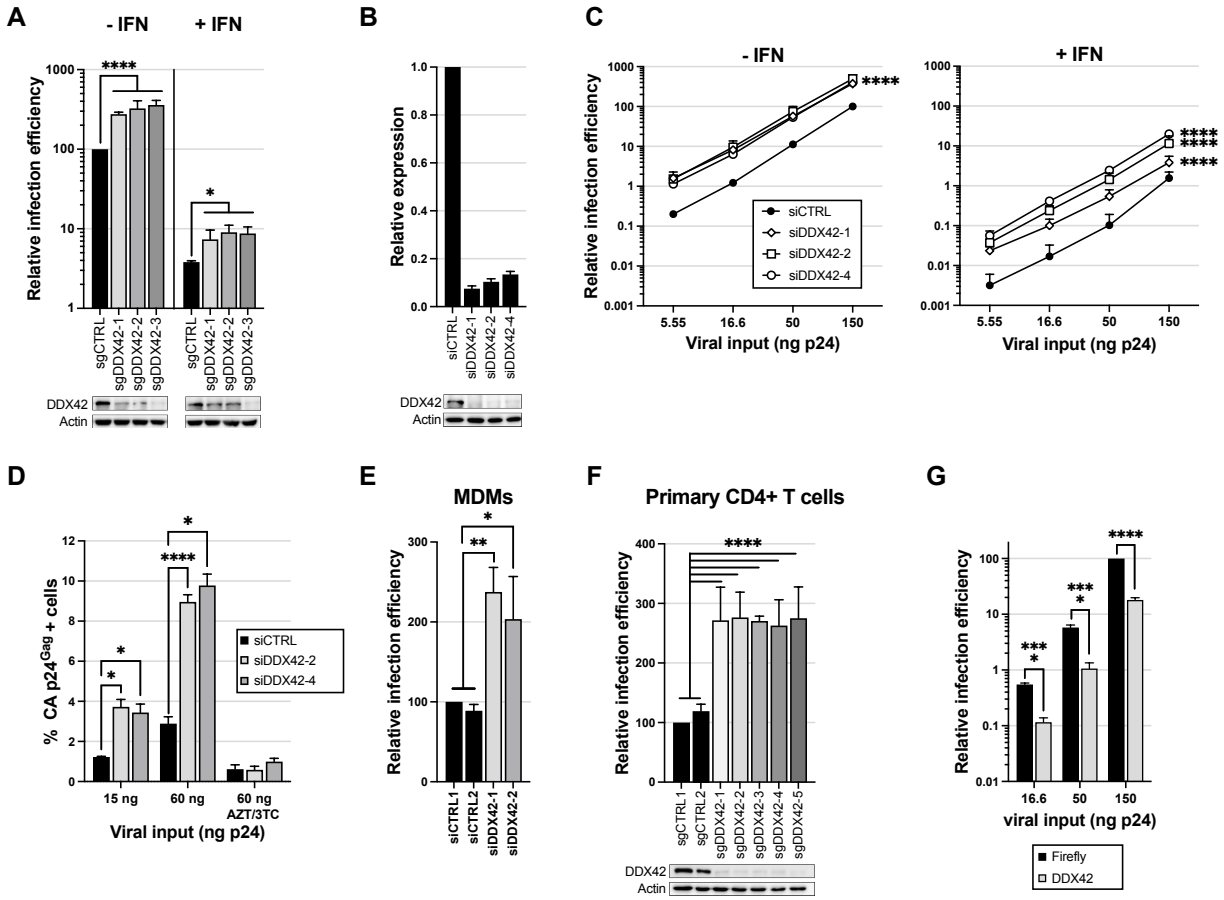

163

164 **Figure 2. DDX42 is an intrinsic inhibitor of HIV-1.**

165 **A**. Top: *DDX42* KO and CTRL KO U87-MG/CD4/CXCR4/Cas9/Firefly cells were generated using 3 sgRNAs and
166 4 non-targeting sgRNAs, respectively (for CTRL, the average of data obtained with 4 cell populations is shown).
167 Cells were treated or not with IFN 24 h prior to infection with HIV-1 Renilla. Relative luminescence results for
168 IFN-treated and -untreated conditions are shown. Two-way ANOVA on log-transformed data with Sidak's test.

169 Bottom: Immunoblot analysis of DDX42 levels is shown for 1 CTRL and DDX42-depleted populations; Actin
170 served as a loading control.
171 **B**. DDX42 silencing efficiency measured by RT-qPCR (top) and immunoblot (bottom) in parallel samples from C.
172 **C**. siRNA-transfected U87-MG/CD4/CXCR4 cells were treated or not with IFN for 24 h prior to infection with HIV-
173 1 Renilla. Relative luminescence results for IFN-treated and -untreated conditions are shown. Multiple linear
174 regression analysis.
175 **D**. DDX42-depleted cells were infected with HIV-1, and infection efficiency was measured by CA $p24^{Gag}$
176 intracellular staining and flow cytometry analysis. When indicated, cells were treated with azidothymidine (AZT)
177 and lamivudine (3TC). Two-way ANOVA on log-transformed data with Dunnett's test.
178 **E.** siRNA-transfected MDMs were infected with a CCR5-tropic version of HIV-1 Renilla. Relative luminescence
179 results from independent experiments performed with cells from 3 donors are shown. Two-way ANOVA on log-
180 transformed data with Dunnett's test.
181 **F**. Primary CD4+ T cells were electroporated with Cas9-sgRNA RNPs using 2 non-targeting sgRNAs (sgCTRL1
182 and 2) and 5 sgRNAs targeting DDX42. Top: Cells were then infected with HIV-1 Renilla and relative infection
183 efficiencies obtained with cells from three donors are shown. Two-way ANOVA on log-transformed data with
184 Dunnett's test. Bottom: DDX42 protein levels were determined by immunoblot, Actin served as a loading control.
185 A representative immunoblot is shown.
186 **G**. Firefly- or DDX42-expresssing U87-MG/CD4/CXCR4 cells were infected with HIV-1 Renilla. Relative infection
187 efficiencies are shown. Multiple linear regression analysis.
188 **A-G** Data represent the mean ± S.E.M of three independent experiments.
189

190 In order to confirm DDX42's effect on HIV-1 infection with an independent approach, we used
191 three different siRNAs to knockdown DDX42 expression. We observed that depleting DDX42
192 (with ~90% efficiency both at the mRNA and protein levels, Fig. 2B) increased HIV-1 Renilla
193 infection efficiency by 3 to 8-fold in U87-MG/CD4/CXCR4 cells, irrespectively of the presence of
194 IFN (Fig. 2C). Of note, wild-type HIV-1 infection was also significantly impacted by DDX42
195 silencing, as measured by Capsid (CA $p24^{Gag}$) intracellular staining 30 h post-infection in U87-
196 MG/CD4/CXCR4 cells (Fig. 2D). We then investigated whether DDX42 had an impact in HIV-1
197 primary target cells. In monocyte-derived macrophages (MDMs), we observed that HIV-1 infection
198 was increased by about 2-fold following DDX42 silencing (Fig. 2E), whereas DDX42 mRNA
199 abundance was decreased by only 40% (Fig. S2B). Electroporation of pre-assembled Cas9-
200 sgRNA ribonucleoprotein complexes (RNPs) was used to efficiently deplete DDX42 in primary
201 CD4+ T cells (Fig. 2F). DDX42 depletion increased HIV-1 infection by 2- to 3-fold, showing a role
202 of DDX42 as an intrinsic inhibitor of HIV-1 in primary CD4+ T cells. Next, we analysed the
203 consequences of DDX42 overexpression on HIV-1 infection. An irrelevant control (Firefly) or

204 DDX42 were ectopically expressed in U87-MG/CD4/CXCR4 and the cells were challenged with
205 HIV-1 (Fig. 2G). DDX42 overexpression induced a substantial inhibition of HIV-1 infection (~5-
206 fold decrease in infection efficiency in comparison to the control). Interestingly, the expression of
207 K303E DDX42 mutant, which is unable to hydrolyse ATP and may supposedly act as a dominant
208 negative[25,26], increased HIV-1 infection by 3-fold, reminiscent of the impact of DDX42 depletion
209 (Fig. S2C). Altogether, these data showed that endogenous DDX42 is able to intrinsically inhibit
210 HIV-1 infection.
211
212 In order to determine which step of HIV-1 life cycle was affected by DDX42, we quantified HIV-1
213 DNA accumulation over time in DDX42-silenced and control cells (Fig. 3A; silencing efficiency is
214 shown in Fig. 3B). DDX42 depletion increased accumulation of early and late reverse transcript
215 products (by 2.5- to 8-fold), as well as proviral DNA and 2-long terminal repeat (2-LTR) circles at
216 48h post-infection (by 2.5- to 4.5-fold). Importantly, DDX42 silencing did not impact HIV-1 entry
217 (Fig. S3A). These data suggested that endogenous DDX42 could inhibit reverse transcription
218 and/or impact genome stability, leading to a decrease in viral DNA accumulation. We
219 hypothesized that if that was the case, DDX42 should be found in close proximity to HIV-1 reverse
220 transcription complexes during infection. In agreement with this, proximity ligation assay (PLA)
221 performed on HIV-1 infected MDMs showed that DDX42 was indeed in close vicinity of Capsid
222 (Fig. 3C).
223
224 We next examined the ability of DDX42 to inhibit infection by various primate lentiviruses,
225 including lab-adapted strains of HIV-1 (NL4-3, IIIB), transmitted/founder strains[27] (CH077.t,
226 CH106.c, REJO.c), HIV-2 and simian immunodeficiency virus from rhesus macaque (SIV_{MAC}).
227 DDX42 was depleted or not in TZM-bl reporter cells prior to infection with VSV-G-pseudotyped
228 lentiviruses, and infection efficiency was monitored 24h later (Fig. 3D; silencing efficiency is
229 shown in Fig. 3E). DDX42 depletion increased infection levels similarly with all the tested strains
230 of HIV-1 (i.e. 3- to 5-fold). HIV-2rod10 and SIV_{MAC} infection efficiencies were also slightly improved
231 in the absence of DDX42 (~2-fold). The analysis was then extended to two non-primate

232 lentiviruses, equine infectious anemia virus (EIAV) and feline immunodeficiency virus (FIV), using
233 GFP-coding LVs in U87-MG cells (Fig. 3F). DDX42 depletion appeared to increase HIV-1, HIV-2
234 and FIV LV infection to the same extent (~2-fold), whereas EIAV infection was less impacted. Of
235 note, DDX42 antiviral activity appeared less potent on HIV-1 LVs compared to full-length HIV-1,
236 which might suggest that genome length or cis-acting elements could play a role in DDX42
237 inhibition. We also observed that DDX42 depletion led to a significant increase in infection with
238 GFP-coding, MLV-derived vectors (Fig. 3G). These results strongly support a general antiviral
239 activity of DDX42 against retroviruses.
240
241 DDX42 can be found in the cytoplasm but is predominantly located in the nucleus in various cell
242 types, including monocyte-derived macrophages[28,29] (Fig. S3B). Considering that DDX42 showed
243 a broad activity against retroviruses and seemed to act at the level of reverse transcription, we
244 sought to investigate whether DDX42 could inhibit retrotransposons. Long interspersed nuclear
245 elements (LINE)-1 are non-LTR retrotransposons, which have been found to be active in the germ
246 line and some somatic cells[30]. Interestingly, DDX42 was identified among the suppressors of
247 LINE-1 retrotransposition through a genome-wide screen in K562 cells, although not further
248 characterized[31]. To confirm that DDX42 could inhibit LINE-1 retrotransposition, HEK293T cells
249 were co-transfected with GFP-expressing LINE-1 plasmids (RPS or LRE3) or an inactive LINE-1
250 (JM111) together with a DDX42- or a control (Firefly)-expressing plasmid[32]. LINE-1
251 retrotransposition was quantified by flow cytometry 7 days later (Fig. 3H). As the GFP cassette is
252 cloned in antisense and disrupted by an intron, GFP is only expressed after LINE-1 transcription,
253 splicing, Orf2p-mediated reverse transcription, and integration[32]. Successful retrotransposition
254 events were observed in >1.25% of control cells, but in only <0.25% of DDX42-expressing cells
255 (i.e. a percentage similar to what observed with the non-active LINE-1), showing that DDX42
256 ectopic expression significantly suppressed LINE-1 retrotransposition. Next, we investigated
257 whether DDX42 could physically interact with LINE-1 RNAs. Cells were co-transfected with GFP-
258 expressing LINE-1 RPS plasmid and either flag-tagged-Firefly or -DDX42. The cells were lysed 4
259 days later and the flagged proteins immunoprecipitated. The immunoprecipitation eluates were

then divided in two; the immunoprecipitated proteins were analysed by immunoblot (Fig. 3I) and their associated RNAs were extracted and analysed by RT-qPCR using LINE-1 specific primers (Fig. 3J). A significant enrichment of LINE-1 RNAs was observed with DDX42 immunoprecipitation as compared to the Firefly negative control, showing that DDX42 could interact with LINE-1 RNAs.

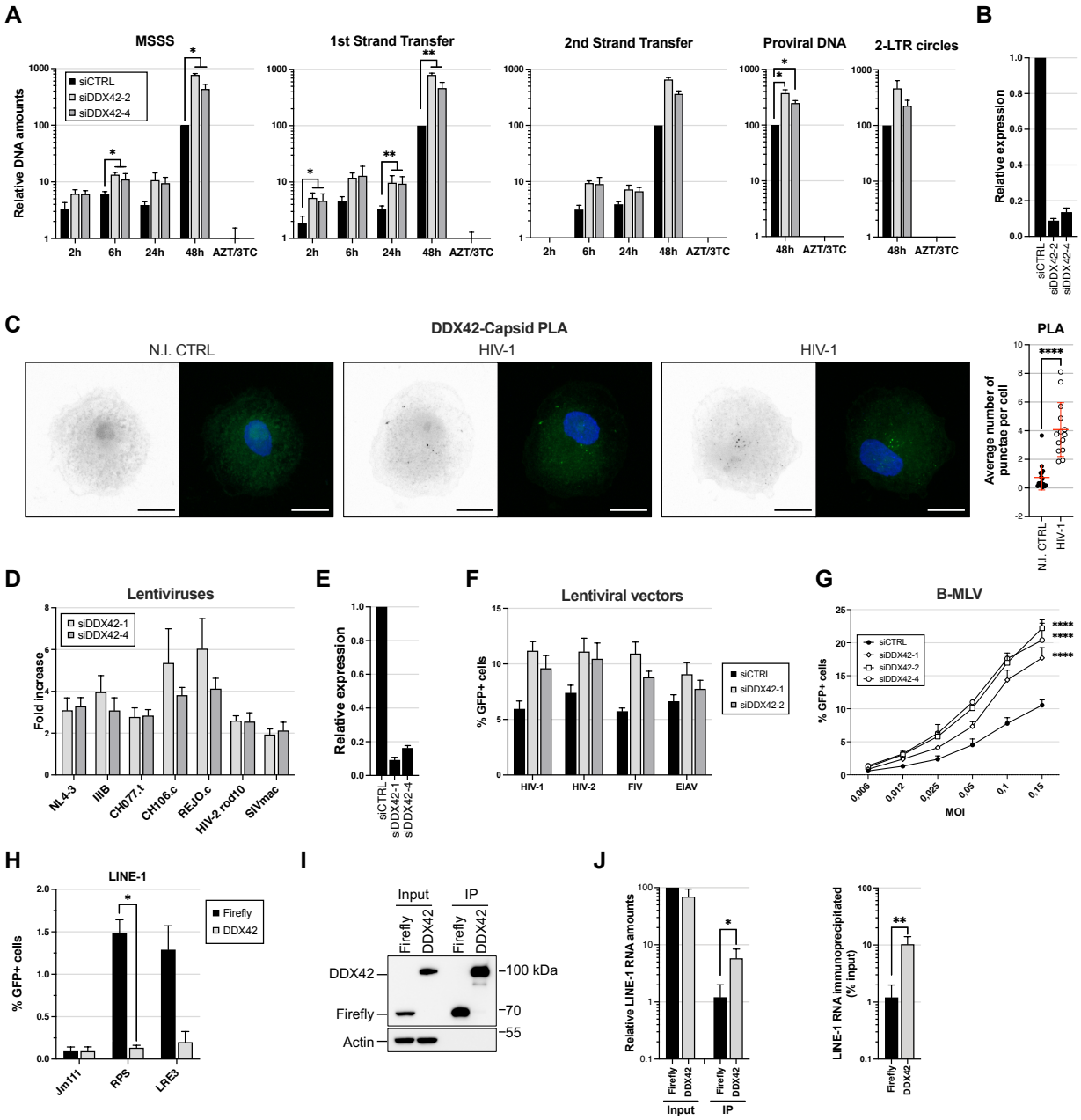

Figure 3. Characterization of DDX42 inhibitory activity against retroviruses and retroelements.

A. siRNA-transfected U87-MG/CD4/CXCR4 cells were infected with HIV-1 and relative amounts of Minus Strand Strong Stop (MSSS), 1st and 2nd Strand Transfer DNAs, and nuclear forms of HIV-1 DNA (proviral DNA, and 2-LTR circles) were quantified by qPCR. DNAs from cells infected for 48 h in the presence of AZT and 3TC were used as a control. Mixed-effects analysis on log-transformed data with Dunnett's test.

271 **B**. Silencing efficiency in parallel samples from A.
272 **C.** PLAs were performed in MDMs infected with HIV-1 or not (N.I. CTRL), using anti-Capsid and anti-DDX42
273 antibodies (nuclei stained with Hoechst). Images were acquired using a LSM880 Airyscan microscope. Left:
274 representative images, scale-bar: 10 μm. Right: Average punctae quantified per cell in 3 independent assays
275 done on MDMs from different donors with mean ± SD (n>65 cells per condition). Mann-Whitney test.
276 **D.** siRNA-transfected TZM-bl cells were infected and β-galactosidase signals measured 24 h later. The ratio of
277 the signal in DDX42-depleted versus CTRL cells is shown.
278 **E**. Silencing efficiency in parallel samples from D.
279 **F.** siRNA-transfected U87-MG/CD4/CXCR4 cells were infected with HIV-1- HIV-2- FIV- EIAV-based, GFP-coding
280 LVs and infection efficiency was scored 24 h later by measuring the percentage of GFP expressing cells by flow
281 cytometry.
282 **G**. siRNA-transfected U87-MG/CD4/CXCR4 cells were infected with GFP-coding B-MLV and infection efficiency
283 measured 24h later by flow cytometry. Simple linear regression analysis.
284 **H**. HEK293T were co-transfected with GFP-coding LINE-1 plasmids (RPS-GFP or LRE3-GFP) or with an inactive
285 LINE-1 plasmid (JM111) together with either a Firefly- or DDX42-coding plasmid. GFP expression was measured
286 by flow cytometry 7 days later. Two-way ANOVA on log-transformed data with Sidak's test.
287 **I**. HEK293T were co-transfected with pRPS-GFP and a Flag-Firefly- (negative control) or Flag-DDX42-coding
288 plasmid, followed by Flag immunoprecipitation and immunoblot analysis. A representative immunoblot is shown.
289 **J**. Left, RNA extraction and LINE-1 RT-qPCR on parallel samples from H. Two-way ANOVA on log-transformed
290 data with Sidak's test. Right, Percentage of immunoprecipitated RNA from I. T-test on log-transformed data.
291 **A-H**. Data represent the mean ± S.E.M of 3 independent experiments. **J**. Data represent the mean ± S.E.M of 5
292 independent experiments.
293

294 Finally, we sought to determine whether DDX42's inhibitory activity was specific towards
295 retroviruses and retroelements, or could be extended to other viruses, as observed for many other
296 anti-HIV-1 proteins, such as ZAP or BST-2/Tetherin[1,8]. To this aim, we tested the impact of DDX42
297 depletion on eight RNA viruses from five different families: the orthomyxovirus influenza A virus
298 (IAV), the rhabdovirus vesicular stomatitis virus (VSV), the paramyxovirus measles virus (MeV),
299 the flaviviruses ZIKV, Dengue virus serotype 2 (DENV-2) and yellow fever virus (YFV), the
300 alphavirus CHIKV, and the coronavirus SARS-CoV-2, which is responsible for the current
301 coronavirus disease (COVID)-19 pandemic (Fig. 4). Strikingly, DDX42 depletion had no
302 significant effect on IAV, VSV and MeV replication in U87-MG and Huh-7 cells, respectively (Fig.
303 4A-C; silencing efficiency is shown in Fig. S4A), thereby strongly suggesting that manipulating
304 DDX42 expression did not have a broad and unspecific impact on target cells. Interestingly,
305 depletion of endogenous DDX42 had a modest but significant, positive impact on ZIKV in U87-

306 MG cells (Fig. 4D), whereas the impact in Huh-7 cells was less important (Fig. S4B and A).
307 Similarly, DDX42 silencing had little effect on 2 other flaviviruses (DENV-2 and YFV) in Huh-7
308 cells, as measured by the number of cells positive for the viral protein E (Fig. S4C-D). By contrast,
309 DDX42 depletion had a profound effect on both CHIKV (Fig. 4E) and RC-2020-00558 SARS-
310 CoV-2 replication (Fig. 4F-G) (up to 1 log- and 3 log-increase in infection efficiency with CHIKV
311 and SARS-CoV-2, respectively; silencing efficiencies in the different cell lines used are shown in
312 Fig. S4A). Plaque assays confirmed a strong impact of DDX42 depletion on infectious SARS-
313 CoV-2 production (Fig. 4G). In agreement with this, DDX42 was recently identified as a potential
314 inhibitor of SARS-CoV-2 replication in a CRISPR screen in simian cells[33]. Next, we used PLA to
315 determine whether DDX42 was in the vicinity of SARS-CoV-2 components in infected cells. To
316 this aim, PLA was performed with either anti-double strand (ds)RNA or anti-Nucleoprotein (N)
317 antibody, together with anti-DDX42 antibody, followed by an immunofluorescence staining to
318 identify the infected cells (Fig. 4H-I). In the latter, there was a significantly higher number of
319 dsRNA-DDX42 and N-DDX42 PLA punctae than in control cells. This suggested a potential
320 interaction between DDX42 and SARS-CoV-2 viral components. To test whether DDX42 RNA
321 helicase could interact with viral RNAs, RNA immunoprecipitation experiments were conducted
322 following viral infection of U87-MG and A549-ACE2 cells expressing either Flag-DDX42 or
323 negative control Flag-Firefly. A significant enrichment of the viral RNAs recovered with Flag-
324 DDX42 was observed in comparison to the negative control, and this was observed for the
325 sensitive viruses SARS-CoV-2 and CHIKV (Fig. 4J-K), but not for IAV, which was insensitive to
326 DDX42 antiviral activity (Fig. 4L and 4A).
327

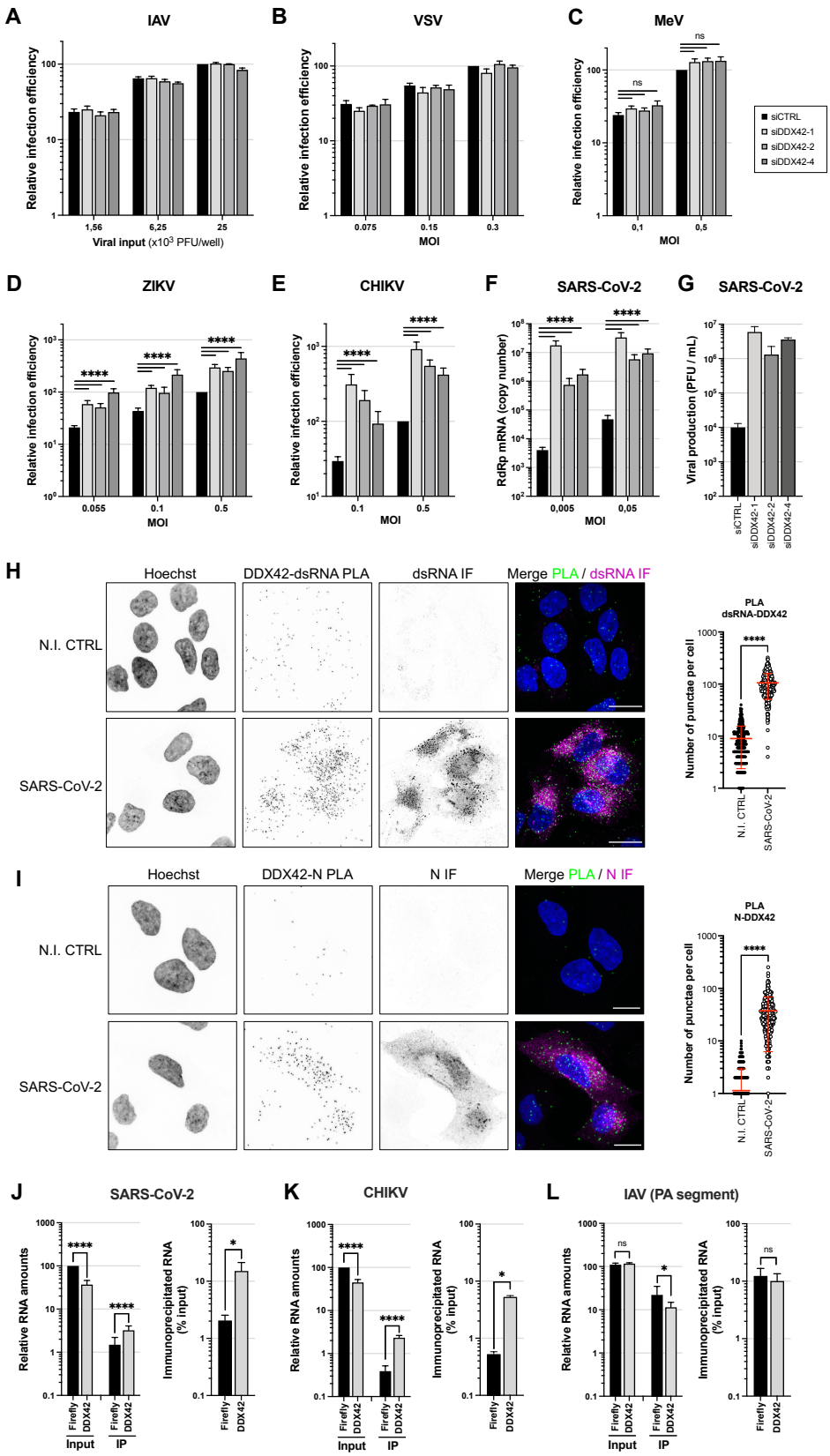

Figure 4. DDX42 exerts a broad antiviral activity on positive strand viruses and interacts with viral RNAs from targeted viruses.

A. Relative IAV infection efficiency in siRNA-transfected U87-MG cells (Nanoluciferase activity 16 h post infection).

333 **B.** Relative VSV infection efficiency in siRNA-transfected U87-MG cells (Firefly activity 24 h post infection).
334 **C.** Relative MeV infection efficiency in siRNA-transfected Huh-7 cells (GFP+ cells scored 24h post infection).
335 Multiple linear regression analysis.
336 **D.** Relative ZIKV infection efficiency in siRNA-transfected U87-MG cells (Nanoluciferase activity 24 h post
337 infection). Multiple linear regression analysis.
338 **E.** Relative CHIKV infection efficiency in siRNA-transfected U87-MG cells (Nanoluciferase activity 24 h post
339 infection). Multiple linear regression analysis.
340 **F.** Relative SARS-CoV-2 infection in siRNA-transfected A549-ACE2 cells (RdRp RT-qPCR 48 h post-infection).
341 Mixed-effects analysis on log-transformed data with Dunnett's test.
342 **G**. Viral production in cell supernatants from F (48 h post-infection, MOI 0,05) measured by plaque assays.
343 **H.** A549-ACE2 cells were infected or not with SARS-CoV-2 for 24 h prior to PLA using mouse anti-dsRNA (J2)
344 and rabbit anti-DDX42 antibodies, followed by additional immunofluorescence (IF) staining with anti-mouse Alexa
345 Fluor 546 antibody (PLA in green, IF in magenta). Representative Z-stack projection images are shown; scale
346 bar: 15 μm. Average punctae were quantified in 3 independent PLA assays with mean ± SD (n>75 cells per
347 condition). Mann-Whitney test.
348 **I**. Identical to H but using an anti-N antibody instead of anti-dsRNA antibody.
349 **J**. Left, Quantification of SARS-CoV-2 RNA by RT-qPCR in RNA from total cell lysates (input) and in Flag-Firefly
350 (negative control) and Flag-DDX42 immunoprecipitation (IP). Multiple linear regression analysis on log-
351 transformed data.
352 Right, Percentage of immunoprecipitated RNA. Paired t-test on log-transformed data.
353 **K**. Identical to J following CHIKV infection.
354 **L**. Identical to J following IAV infection.
355 Data represent the mean ± S.E.M. of three (**A-E, J-L**), four (**F**) or two (**G**) independent experiments.
356

357 As mentioned above, DDX42's lack of effect of negative strand RNA viruses argued against a
358 global, indirect effect on the target cells. However, to confirm this, we performed RNA-seq
359 analysis on siRNA-treated U87-MG and A549-ACE2 cells. The results showed that DDX42
360 depletion didn't have a substantial impact on global cellular RNA expression (Supplementary File
361 1 and Fig. S5). Of note, only 63 genes were commonly found differentially expressed upon DDX42
362 depletion with the 3 different siRNAs in U87-MG cells, and only 23 genes were identified in
363 common in U87-MG and A549-ACE2 cells (differentially expressed genes, DEGs, with a fold
364 increased ≥ 2 and an adjusted p-value < 0.05). Importantly, no known restriction factors were
365 identified among the DEGs (Supplementary File 1). Taken together, these data strongly
366 suggested that the DEAD-box RNA helicase DDX42 directly impacted viral replication, by
367 interacting with viral RNAs.
368

369 **Discussion**

370 Here, we identified for the first time the RNA helicase DDX42 as an intrinsic inhibitor of HIV-1,
371 capable of limiting the efficiency of viral DNA accumulation. Moreover, our study revealed broad
372 activity of endogenous DDX42 against retroviruses and retroelements, which was observed in
373 various cell types, including primary CD4+ T cells. Strikingly, we observed that DDX42 was able
374 to inhibit viruses from other families, which possess different replication strategies, including
375 SARS-CoV-2 and CHIKV. However, DDX42 did not have an impact on all the viruses we tested,
376 as three different negative-strand RNA viruses were found insensitive to DDX42 antiviral activity.
377 This is reminiscent of other broad-spectrum antiviral inhibitors such as MX1, which show some
378 specificity despite being able to inhibit viruses from various families[34]. Further work is now
379 warranted to explore in depth the breadth of DDX42 antiviral activity and determine whether it is
380 truly specific of positive strand RNA viruses.

381 Interestingly, our PLA assays showed a close proximity between DDX42 and HIV-1 Capsid, which
382 is a viral protein recently shown to remain associated with reverse transcription complexes until
383 proviral DNA integration in the nucleus[35–37]. We also observed a close proximity between DDX42
384 and SARS-CoV-2 N or dsRNA. Furthermore, LINE-1 RNAs, as well as SARS-CoV-2 and CHIKV
385 RNAs, were specifically pulled-down when DDX42 was immunoprecipitated. Taken together,
386 these observations strongly suggest a direct mode of action of DDX42, which could interact with
387 target viral RNAs. DDX42 is known to be a non-processive helicase, which also possesses RNA
388 annealing activities and the ability to displace RNA-binding proteins from single-stranded RNAs[23].
389 Moreover, DDX42 binds G-quadruplexes[38], which are secondary structures found in cellular and
390 viral nucleic acids and involved in various processes, such as transcription, translation and
391 replication[39,40]. All these known activities of DDX42 would be consistent with a potential role in
392 RNP remodeling[23,41]. Nonetheless, further investigation will be needed to determine whether
393 DDX42 acts directly by altering viral RNPs, and, if that's the case, what are the determinants for
394 viral RNP recognition.

395 In conclusion, this work highlights the importance of understanding the mechanism of action of
396 DDX42 RNA helicase and its contribution to the control of RNA virus replication, an understanding
397 which may contribute to the development of future antiviral interventional strategies.

398 **Methods**

399

400 **Plasmids.** The pLentiCas9-Blast, pLentiGuide-Puro vectors and the GeCKO sub-library A and B
401 plasmids were a gift from Prof. F. Zhang (Addgene #52962, #52963, and #1000000048,
402 respectively[17]). LVs coding for sgRNAs targeting the candidate genes and control genes were
403 obtained by cloning annealed oligonucleotides in BsmBI-digested pLentiGuide-Puro, as
404 described (Addgene). Control sgRNAs and sgRNAs targeting the candidate genes, *MX2* and
405 *IFNAR1*, were designed with the Optimized CRISPR Design tool (not available anymore), or with
406 Chopchop (chopchop.cbu.uib.no). The sgRNA coding sequences used were as follow: MX2 5'-
407 CCGCCATTCGGCACAGTGCC-3', IFNAR1 5'-GACCCTAGTGCTCGTCGCCG-3', sgCTRL-1 5'-
408 AGCACGTAATGTCCGTGGAT-3', sgCTRL-2 5'-CAATCGGCGACGTTTTAAAT-3', sgCTRL-3
409 5'-TTAATTTGGGTGGGCCCTGC-3', sgCTRL-4 5'-TTGGATATTAATTAGACATG-3', sgDDX42-
410 1 5'-TCCTGAACCACACCAGCAGT-3', sgDDX42-2 5'-GGTGGTCCTGGCACTAAGCG-3',
411 sgDDX42-3 5'-AGGCACTGTGGGACTGCTGT-3'. All the other sgRNA sequences are available
412 upon request. In order to produce the HIV-1 based LVs used to perform the different steps of the
413 screen (pRRL.sin.cPPT.CMV/NeomycinR.WPRE, pRRL.sin.cPPT.CMV/HygromycinR.WPRE
414 and pRRL.sin.cPPT.CMV/ZeocinR.WPRE), neomycin, hygromycin and zeocin resistance genes
415 (i.e. the genes coding for Neomycin phosphotransferase II, Hygromycin B phosphotransferase,
416 and *Sh ble*) were amplified by PCR from pcDNA3.1 (ThermoFisher Scientific), pAHM[11], and
417 pcDNA3.1/Zeo (ThermoFisher Scientific), respectively, and cloned by replacement of GFP in
418 pRRL.sin.cPPT.CMV/GFP.WPRE[42] using BamHI and SalI restriction sites. The
419 pRRL.sin.cPPT.SFFV/E2-crimson-IRES-PuromycinR.WPRE has been described[43]. Human
420 DDX42 cDNA was amplified by RT-PCR using the SuperScript III™ (Invitrogen) from mRNAs of
421 MDMs using primers DDX42-forward 5'-
422 AATTAATTTAGGATCCATGAACTGGAATAAAGGTGGTCCTG and DDX42-reverse 5'-
423 AATTAATTTACTCGAGCTAACTGTCCCATCGACTTTTCTTGCG, and cloned by replacement of
424 E2-crimson in BamHI-XhoI-digested pRRL.sin.cPPT.SFFV/E2crimson-IRES-
425 PuromycinR.WPRE, in order to obtain pRRL.sin.cPPT.SFFV/DDX42-IRES-PuromycinR.WPRE.

426 The pRRL.sin.cPPT.SFFV/CD4-IRES-CXCR4.WPRE was obtained by replacement of E2-
427 crimson-IRES-PuroR in pRRL.sin.cPPT.SFFV/E2-crimson-IRES-PuromycinR.WPRE with a
428 BamHI/SalI fragment digested CD4-IRES-CXCR4 PCR fragment obtained from pMLV-CD4-
429 IRES-CXCR4 (a gift from Prof. N. Sherer, Wisconsin University, USA).
430 pRRL.sin.cPPT.SFFV/Firefly-IRES-PuromycinR.WPRE was obtained by amplification of Firefly
431 by PCR from pGL4 (Promega) and cloned into BamHI-XhoI-digested pRRL.sin.cPPT.SFFV/E2-
432 crimson-IRES-PuromycinR.WPRE. In some experiments, LVs without a selection marker were
433 used: the IRES-PuromycinR cassette was removed by XhoI-SalI digestion and subsequent
434 ligation, to obtain pRRL.sin.cPPT.SFFV/Firefly.WPRE and pRRL.sin.cPPT.SFFV/DDX42.WPRE.
435 DDX42 K303E mutant was obtained by site-directed mutagenesis (by overlapping PCR using the
436 aforementioned DDX42-forward and -reverse primers, respectively combined initially with reverse
437 primer 5'-GGCTGCAGTTTCCCCACTACCTGTTTTGGCAATACC and forward primer 5'-
438 GGTAGTGGGGAAACTGCAGCCTTCATTTGGCC). pRRL.sin.cPPT.SFFV/ACE2.WPRE has
439 been described[44] (Addgene 145842). Flag-DDX42 and Flag-Firefly were amplified by PCR from
440 the aforementioned LV plasmids and cloned into a NotI-XhoI-digested modified version of
441 pCAGGS[45] to obtain pCAGGS/flag-DDX42.WPRE and pCAGGS/flag-Firefly.WPRE. The NL4-
442 3/Nef–internal ribosome entry signal (IRES)-Renilla (NL4-3/Nef-IRES-Renilla) and the CCR5-
443 version of this proviral clone were gifts from Prof. Sumit Chanda[20]. Wild-type and Ba-L Env
444 bearing HIV-1 NL4-3, IIIB and HIV-2 proviral clones have been described[46–48], as well as the
445 transmitted founder HIV-1 molecular clones CH077.t, CH106.c, REJO.c (gifts from Prof. B.
446 Hahn[27]) and HIV-2_{ROD10} and SIV_{MAC239}[49,50]. GFP-coding HIV-1 based LV system (i.e. p8.91 HIV-1
447 Gag-Pol, pMD.G, and GFP-coding minigenome), and HIV-2, FIV, and EIAV-derived, GFP coding
448 LVs, as well as MLV-derived, GFP coding retroviral vectors have all been described[51,52,53,54]. The
449 LINE-1 plasmid 99 RPS-GFP PUR (pRPS-GFP), 99 RPS-GFP JM111 PUR (pJM111) and
450 pLRE3-GFP were developed by Prof. Kazazian's lab[32,55,56].
451
452 **Cell lines.** Human cell lines HEK293T, A549, U87-MG, TZM-bl were obtained from the ATCC
453 and the AIDS reagent program, respectively. T98G cells were a gift from Prof. G. Kochs (Freiburg

454 University, Germany), MDCK cells a gift from Prof. W. Barclay (Imperial College London, UK),
455 Vero E6 cells (Merck) were a gift from Christine Chable (CEMIPAI, CNRS). Human hepatocellular
456 carcinoma Huh-7 cells[57] were kindly given by Annette Martin (Institut Pasteur, Paris). These cell
457 lines were cultured in Dulbecco's Modified Eagle Medium (DMEM) supplemented with 10% fetal
458 bovine serum and 1 % penicillin-streptomycin (Thermofisher). T98G/Cas9 and U87-MG/Cas9
459 were obtained by transduction of T98G and U87-MG, respectively, with HIV-1-based LVs
460 expressing the spCas9-P2A-Blasticidin cassette (pLentiCas9-Blast[17]). U87-MG/CD4/CXCR4
461 have been described [11] and were further modified to express Cas9 and Firefly using pLentiCas9-
462 Blast and pRRL.sin.cPPT.SFFV/Firefly.WPRE, respectively. T98G/Cas9/CD4/CXCR4/Firefly
463 were obtained by successive transductions of T98G/Cas9 with pRRL.sin.cPPT.SFFV/CD4-IRES-
464 CXCR4.WPRE at a high MOI, and pRRL.sin.cPPT.SFFV/Firefly.WPRE, at a low MOI,
465 respectively. Cell surface staining with anti-CD4 and CXCR4 antibodies (Miltenyi Biotec)
466 confirmed than more than 95% cells were positive for both markers. A549 cells stably expressing
467 ACE2 were generated by transduction with RRL.sin.cPPT.SFFV.ACE2.WPRE containing-vector.
468 For antibiotic selection, cells were treated with 10 μg/mL Blasticidin (InvivoGen), 1 mg/mL Zeocin
469 (InvivoGen), 2 μg/mL Puromycin (Sigma-Aldrich), 250 μg/mL Hygromycin (Sigma-Aldrich), 1
470 mg/mL G418 (Sigma-Aldrich). When indicated, universal type 1 IFN (PBL Interferon Source) was
471 added at 1000 U/mL for 16-24h prior to virus infection or RNA extraction, and AZT and 3TC (AIDS
472 reagent program) at 10 μM for 2 h prior to infection.
473
474 **Primary cells.** Blood from healthy donors was obtained from the Etablissement Français du
475 Sang, under agreement n°21PLER2019-0106. Peripheral blood mononuclear cells (PBMCs)
476 were isolated by centrifugation through a Ficoll® Paque Plus cushion (Sigma-Aldrich). Primary
477 human CD4+ T cells and monocytes were purified by positive selection using CD3 and CD14
478 MicroBeads, respectively (Miltenyi Biotec), as previously described[11]. Monocytes were incubated
479 for 3 hours in serum-free Roswell Park Memorial Institute (RPMI) 1640 medium and further
480 differentiated into macrophages by culture for 5-7 days in RPMI 1640 supplemented with 10%

481 fetal calf serum, 1% penicillin-streptomycin and 100 ng/ml granulocyte-macrophage colony-
482 stimulating factor (GM-CSF; Miltenyi). CD4+ T cells were cultured in RPMI supplemented with
483 10% fetal bovine serum and 1% penicillin-streptomycin, and stimulated for 48h with 10 µg/ml
484 phytohemagglutinin (PHA) (Fisher Scientific) and 50 U/mL interleukin-2 (IL-2, Miltenyi Biotec)
485 prior to electroporation.
486
487 **Genome-scale CRISPR/Cas9 screens**. The plasmids coding GeCKO sub-libraries A and B were
488 amplified and prepared according to the provided guidelines (Lentiviral Crispr Toolbox, Addgene).
489 60 million T98G/Cas9 cells were transduced with GeCKO LVs at a MOI of 0,1 to cover about 100-
490 times the half-library complexity. After 48h, the cells were selected with puromycin, amplified for
491 12-15 days. 45 million cells were harvested and frozen down at -80°C for subsequent genomic
492 DNA extraction, using the QIAamp DNA Blood Maxi Kit according to manufacturer's instructions
493 (Qiagen). In parallel, 60 million cells from the initial GeCKO populations were used for the screen.
494 The cells were treated with 1000 U/mL IFN for 24h, infected with LVs coding a hygromycin
495 resistance cassette. 48h later the cells selected with hygromycin and the surviving cells amplified.
496 Two other rounds of IFN treatment, LV infection and antibiotic selection were subsequently
497 performed with LVs coding a neomycin resistance cassette and a zeocin resistance cassette,
498 respectively. The three time-selected populations were amplified and 45 million cells were
499 harvested and stored at -80°C for subsequent genomic DNA extraction, as previously. After
500 genomic DNA extraction, the sgRNA coding sequences integrated in the genomic DNA from the
501 initial and 3-times selected populations were amplified by touch-down PCR and sequenced by
502 Illumina deep sequencing. To this aim, 120 µg of genomic DNA was amplified using DNA
503 Herculase II Fusion DNA polymerase (Agilent) in the presence of 2% DMSO, 1 mM of dNTPs;
504 and 400 nM of the following primers: Forward-primer1: 5'-
505 TCGTCGGCAGCGTCAGATGTGTATAAGAGACAGCTTGTGGAAAGGACGAAACACC-3' for
506 screen A or Forward-primer2: 5'-
507 TCGTCGGCAGCGTCAGATGTGTATAAGAGACAGGATCTTGTGGAAAGGACGAAACACC-3'
508 used for screen B, together with reverse primer: 5'-

509 GTCTCGTGGGCTCGGAGATGTGTATAAGAGACAAAGGTCCATTAGCTGCAAAGATTCCTCT
510 C-3'). Briefly, after 5 minutes at 95°C, 14 cycles of pre-amplification were performed with a
511 hybridization temperature decreasing by 0.5°C per cycle (30 sec at 95°C, 30 sec at 60°C, 30 sec
512 at 72°C), followed by 30 cycles of amplification (30 sec at 95°C, 30 sec at 53°C, 30 sec at 72°C).
513 50 ng of each amplicon was dual indexed in a 5-cycle PCR reaction using the PCR module and
514 indexed primers from the Nextera kit (Illumina). Resulting libraries were purified on AMPure XP
515 magnetic beads (Beckman Coulter) using a 0,8X ratio and verified on Fragment Analyzer using
516 the HS NGS fragment kit (Agilent). Libraries were quantified using microfluorimetry (QuBit,
517 Invitrogen), mixed with a PhiX library (Illumina) and sequenced on one single read 50nt lane of
518 Hiseq2500 using the rapid mode.
519 Image analyses and base calling were performed using the Illumina HiSeq Control Software and
520 Real-Time Analysis component (v1.18.66.3). Demultiplexing was performed using Illumina's
521 conversion software (bcl2fastq 2.20). The quality of the raw data was assessed using FastQC
522 (v0.11.5) from the Babraham Institute and the Illumina software SAV (Sequencing Analysis
523 Viewer). Potential contaminants were investigated with the FastQ Screen[58] (v0.11.4) software
524 from the Babraham Institute.
525 Sequencing reads were trimmed using Cutadapt[59] (v1.13), with options -g [primer sequence] -u
526 [length of remaining 3' bases] -e 0.2 -m 18 -l 20, to remove primer sequences and retrieve the 20
527 bases long sequences corresponding to sgRNAs. These retrieved sequences were then aligned
528 to the GecKOv2 Human Library (A or B) reference sequences (keeping only non-duplicated
529 sgRNA sequences, the duplicated ones being annotated) using Bowtie[60] (v1.2), with options -v 2
530 -norc -S. Resulting bam files were sorted and indexed using Samtools[61] (v1.5). Quantification of
531 sgRNAs was done using Samtools idxstats. MAGeCK[18] (v0.5.7) was used to normalize (total
532 count method) and identify enriched sgRNAs and genes in 3-times selected cell populations
533 versus starting GeCKO transduced cells (mageck test command).
534
535 **Lentiviral and retroviral production.** To produce lentiviral vector particles, HEK293T cells were
536 transfected by polyethylenimine (PEI) co-transfection with miniviral, HIV-1 based genome coding

537 plasmids (e.g. LentiCas9-Blast, LentiGuide-Puro or pRRL-SFFV), p8.91 (HIV-1 GagPol) and
538 pMD.G (VSV-G) at a ratio of 1:1:0.5, respectively. The medium was replaced after 6h and viral
539 particles were harvested 42h later, filtered, and directly used to transduce target cells (or stored
540 at -80°C). After 4 to 6 hours, the transduction medium was replaced with complete DMEM, and
541 the cells were treated 48h later with the relevant antibiotics. The HIV-2-, FIV-, EIAV-GFP coding
542 LVs were produced using GFP-coding HIV-2-, FIV-, EIAV-based miniviral genomes, together with
543 HIV-2-, FIV-, EIAV- GagPol, expression constructs and pMD.G at a ratio of 1:1:0.5. MIGR1 MLV-
544 derived retroviral vectors were obtained with B-MLV Gag-Pol-expressing plasmid pCIG3B, the
545 GFP-expressing minigenome pMIGR1 and pMD.G. at a ratio of 1:1:0.5, respectively and
546 harvested as previously described.
547 HIV-1 Renilla and NL4-3 HIV-1 were produced by standard PEI transfection of HEK293T. When
548 indicated, pMD.G was cotransfected with the provirus at a 3:1 ratio. The culture medium was
549 changed 6h later, and virus-containing supernatants were harvested 42h later. Viral particles were
550 filtered, purified by ultracentrifugation through a sucrose cushion (25% weight/volume in Tris-
551 NaCl-EDTA buffer) for 75 min at 4°C and 28,000 rpm using a SW 32 TI rotor (Beckman Coulter),
552 resuspended in serum-free RPMI 1640 or DMEM medium and stored in small aliquots at -80°C.
553 Viral particles were titrated using an HIV-1 $p24^{Gag}$ Alpha-Lisa kit and an Envision plate reader
554 (Perkin Elmer) and/or by determining their infection titers on target cells.
555
556 **Lentiviral and retroviral infections.** For infections with replication-competent HIV-1 Renilla or
557 wild-type and/or VSV-G pseudotyped-HIV-1, target cells were plated at 2.5 x 10^4 cells per well in
558 96-well plates or at 2 x 10^5 cells per well in 12-well plates and infected for 24-48 h before lysis
559 and Renilla (and Firefly) luciferase activity measure (Dual-Luciferase® Reporter Assay System
560 Promega) or fixation with 2% paraformaldehyde (PFA)-PBS, permeabilization (Perm/Wash buffer,
561 BDBiosciences) and intracellular staining with the anti-$p24^{Gag}$ KC57-FITC antibody (Beckman
562 Coulter), as described previously[62]. For TZM-bl assays, the β-galactosidase activity was
563 measured using the Galacto-Star™ system (ThermoFisher Scientific). For infections with lentiviral
564 and retroviral vectors, target cells were plated at 2.5 x 10^4 cells per well in 96-well plates the day

565 prior to infection with vectors at the indicated MOIs, and the percentages of infected cells were
566 scored by flow cytometry 24h later. For primary CD4+ T cell infections, 10^5 cells were infected
567 with 100 ng $p24^{Gag}$ of HIV-1 Renilla for 24 h prior to lysis and luciferase activity measure. For
568 MDM infections, 8 x 10^4 cells were infected with 100 ng $p24^{Gag}$ of a CCR5-tropic version of HIV-
569 1 Renilla for 30 h prior to lysis and luciferase activity measure.
570
571 **Retrotransposon assays.** For GFP-based retrotransposon assays, HEK293T cells (2 x 10^5 cells)
572 were co-transfected with either 1 µg of pJM111 (a negative control with two point mutations in
573 ORF1 that abolish retrotransposition), pRPS-GFP or pLRE3-GFP with either 1 µg of pCAGGS-
574 Flag-Firefly or pCAGGS-Flag-DDX42. At 7 days post-transfection, the percentage of GFP-
575 expressing cells was scored by flow cytometry.
576
577 **CRISPR/Cas9 knock-out.** For CRISPR/Cas9 knock-out in cell lines, Lentiguide-Puro LVs coding
578 sgRNAs targeting the indicated genes or non-targeting sgRNAs were produced, and U87-MG
579 Cas9/CD4/CXCR4/Firefly were transduced for 6 h before replacing the supernatants with fresh,
580 complete medium. The transduced cells were selected with puromycin two days later and
581 amplified for 12-15 days. For CRISPR/Cas9 knock-out in activated primary CD4+ T cells, 2 million
582 cells per condition were washed with PBS1X, and electroporated using the 4d-Nucleofector®
583 (Lonza) and the Amaxa P3 primary cell kit with 183 pmol of crispr/tracr RNA duplex (Alt-R
584 CRISPR-Cas9 crRNA XT and tracrRNA XT, IDT®) and 61 pmol of Cas9 (Alt-R® S.p. Cas9
585 Nuclease V3, IDT®). After electroporation, the cells were incubated for 4 days at 37°C in X-
586 VIVO15 medium (Lonza) supplemented with 1% pen/strep and IL-2 at 500 U/ml prior to cell
587 counting and infection. The crRNA sequences of the sgDDX42-1, -2, and -3 were identical to the
588 ones cloned in pLentiguide-Puro, and the crRNA of the sgDDX42-4 and sgDDX42-5 were pre-
589 designed by IDT®, as follow: sg4-DDX42 5'-CGGAGATCTATTAACTGCTG-3', sg5-DDX42 5'-
590 GAGTTGGTGAGTTTTCAGC-3'.
591

592 **siRNA transfection.** DDX42 and control knockdowns were achieved by transfecting the indicated
593 siRNAs at 44nM, 14.2nM, and 100nM final in U87-MG and Huh-7 cells, TZM-bl cells and MDMs,
594 respectively, with lipofectamine RNAimax (Thermofisher Scientific) according to the
595 manufacturer's instructions. The scramble siRNA controls used were universal siCTRL1 (SIC001)
596 and siCTRL2 (SIC002) (Sigma-Aldrich) and the sequences of the siRNAs targeting DDX42 were
597 siDDX42-1: 5'-CAGAAUGCCUGGUUUCGGA-3' (SASI_Hs01_00119846, Sigma-Aldrich®),
598 siDDX42-2: 5'-CUUACCUUGUGUUUGAUGA-3' (SASI_Hs01_00119845, Sigma-Aldrich®),
599 siDDX42-4: 5'-AUCUCGAAUACCCUUUACG-3' (ID :136410, Ambion®).
600
601 **RNA immunoprecipitation.** For LINE-1 RNA immunoprecipitation, HEK293T cells were co-
602 transfected with equal amounts of pRPS-GFP and pCAGGS-Flag-DDX42 or -Flag-Firefly. For
603 viral RNA immunoprecipitation, U87-MG cells were transduced with either Flag-Firefly or Flag-
604 DDX42 coding lentiviral vectors (pRRL.sin.cPPT.SFFV/Flag-Firefly.WPRE and
605 pRRL.sin.cPPT.SFFV/Flag-DDX42.WPRE, respectively) and infected with CHIKV at MOI 0.1,
606 SARS-CoV-2 at MOI 0.13, or A/Victoria/3/75 IAV at MOI 0.1 for 24 h. 4 days post LINE-1-
607 transfection or 24 h post-infection, cells were washed twice in PBS1X, incubated for 10 min with
608 0,1% formaldehyde in PBS1X, for 5 min in 250 mM Glycine and washed twice in cold PBS1X.
609 Cells were lysed in RIPA buffer (50 mM Tris/HCl pH 7.5, 150 mM NaCl, 1% NP-40, 0.5% sodium
610 deoxycholate, 1 mM EDTA, protease inhibitor cocktail and 40 U/mL RNasin). The lysates were
611 clarified by centrifugation at 16,000*g*, for 10 min at 4 °C. Fractions of cell lysates were harvested
612 at this stage to serve as controls for protein and RNA inputs (15%) and the rest was incubated
613 with Flag-magnetic beads (ThermoFisher Scientific) for 2 h at 4 °C. The beads were washed 5
614 times in RIPA buffer and the immunoprecipitated proteins eluted using 150 µg/mL 3x Flag peptide
615 (Sigma-Aldrich) in elution buffer (50 mM Tris/HCl pH 7.5, 75 mM NaCl, 1mM DTT, protease
616 inhibitor cocktail and 40 U/mL RNasin) for 2 h. Fractions of eluates were harvested for immunoblot
617 analysis (1/6th) and the rest subjected to RNA extraction (5/6th). RNA extractions were then
618 performed using TRIzol (ThermoFisher Scientific).
619

620 **RNA quantification by RT-qPCR.** To check silencing efficiency or measure gene induction after
621 IFN treatment, 0,5-2 x 10^6 cells were collected 2-3 days after siRNA transfection or 24h after IFN
622 treatment or no treatment, and total RNAs were isolated using the RNeasy kit with on-column
623 DNase treatment (Qiagen). cDNAs were generated using 250 ng RNA (High-Capacity cDNA
624 Reverse Transcription Kit, Applied Biosystem, ThermoFisher Scientific, catalogue number
625 4368814) and analysed by quantitative (q)PCR using TaqMan gene expression assays (Applied
626 Biosystem) specific for ACTB (Hs99999903_m1), GAPDH (Hs99999905_m1), and DDX42
627 (Hs00201296_m1). Triplicate reactions were run according to the manufacturer's instructions
628 using a ViiA 7 Real-Time PCR system. For relative quantification, samples were normalized to
629 both ACTB and GAPDH mRNA expression and ΔΔCt analysis was performed.
630 For the measure of LINE-1 RNAs, 100 ng RNA (from cell extracts) or 25 μl of RNA extracted from
631 the IP eluates (i.e. ~60% of the total amount of immunoprecipitated RNA) were reverse
632 transcribed and analysed by qPCR using primers and probe specific for *ORF2*: ORF2-forward 5'-
633 CACCAGTTAGAATGGCAATCATTAAA-3', ORF2-reverse 5'-GGGATGGCTGGGTCAAATGG-3'
634 with ORF2-probe 5'-[FAM]-AGGAAACAACAGGTGCTGGAGAGGATGC-[TAMRA]-3. Absolute
635 quantification was performed using a pRPS-GFP standard curve.
636 For the measure of SARS-CoV-2 replication, 3 x 10^5 cells were harvested and total RNA was
637 extracted using the RNeasy kit (Qiagen) employing on-column DNase treatment. 125 ng of
638 cellular RNAs were used to generate cDNAs that were analysed by qPCR using RdRp primers
639 and probe, as follow: RdRp_for 5'-GTGARATGGTCATGTGTGGCGG-3', RdRp_rev 5'-
640 CAAATGTTAAAAACACTATTAGCATA-3', and RdRp_probe 5'-[FAM]-
641 CAGGTGGAACCTCATCAGGAGATGC-[TAMRA]-3'[63]. pRdRp (which contains an RdRp
642 fragment amplified from SARS-CoV-2-infected cell RNAs[44]) was diluted in 20 ng/ml salmon sperm
643 DNA to generate a standard curve to calculate relative cDNA copy numbers and confirm the assay
644 linearity (detection limit: 10 molecules of RdRp per reaction).
645 For the measure of the amounts of viral RNAs in the RNA immunoprecipitation experiments, 100
646 ng RNA from cell lysates (input) or 25 μl of RNA extracted from the IP eluates (i.e. ~60% of the
647 total amount of immunoprecipitated) were reverse transcribed using the High-Capacity cDNA

648 Reverse Transcription Kit as above. For SARS-CoV-2, the cDNAs were analysed by RdRp RT-
649 qPCR. For CHIKV RNA, the following primers and probe were used for the qPCR reactions: E1-
650 C21-forward 5'-ACGCAGTTGAGCGAAGCAC-3', E1-C21-reverse 5'-
651 CTGAAGACATTGGCCCCAC-3'[64], and E1-C21-probe 5'-[FAM]-
652 CTCATACCGCATCTGCATCAGCTAAGCTCC-[TAMRA]-3'. pE1 (which contains an E1 fragment
653 amplified from CHIKV-infected cell RNAs using primers E1-C21 forward and E1-C21 reverse and
654 cloned into pPCR-Blunt II-TOPO) was used to generate a standard curve and ensure the linearity
655 of the assay (detection limit: at least 10 molecules per reaction). For A/Victoria/3/75 IAV RNA, the
656 following primers and probe, specific for the PA segment, were used, as follow: PA-forward 5'-
657 TTGCTGCACAGGATGCATTA-3', PA-reverse 5'- AGATTGGAGAAGACGTGGCT-3' and PA-
658 probe 5'-[FAM]- TGGCTCTGCAATGGGACACCTCTGC-[TAMRA]-3'. pPolI-RT-Victoria-PA [65]
659 was used to generate a standard curve and ensure the linearity of the assay (detection limit: at
660 least 10 molecules per reaction).
661
662 **Quantification of HIV-1 DNAs.** To measure HIV-1 cDNAs, 2 x 10^5 cells transfected with a control
663 siRNA or siRNAs targeting DDX42 were plated in 24-well plates, and treated or not with 10 μM
664 AZT and 3TC 1-2 h prior to infection. The cells were infected with NL4-3 HIV-1 (60 ng $p24^{Gag}$) for
665 2 h at 37°C, washed with PBS1X and incubated in complete DMEM before being harvested at
666 the indicated times. Cell pellets were frozen at -80°C after two washes in PBS1X. Total DNA
667 extraction was performed using the DNeasy kit (Qiagen) according to the manufacturer's
668 instructions, and a DpnI-treatment step was performed prior to qPCR. Strong stop reverse
669 transcription products were detected using forward primer oHC64 5'-
670 TAACTAGGGAACCCACTGC-3' and reverse primer oHC65 5'-GCTAGAGATTTTCCACACTG-
671 3', 2nd strand transfer product using oHC64 and oSA63R 5'-
672 CTGCGTCGAGAGATCTCCTCTGGCT-3', together with oHC66 probe 5'-[FAM]-
673 ACACAACAGACGGGCACACACTA-[TAMRA]-3'. 2-LTR circular forms were detected using
674 2LTR-forward 5'-GTAACTAGAGATCCCTCAG-3' and 2LTR-reverse 5'-
675 TGGCCCTGGTGTGTAGTTC-3' together with 2LTR-probe 5′-[FAM]-

676 CTACCACACACAAGGCTACTTCCCTGAT-[TAMRA]-3'. Integrated viral DNA was analysed
677 using an Alu qPCR as described before[11]. Briefly, a preamplification of 16 cycles was performed
678 (15 sec at 94°C, 15 sec at 55°C, 100 sec at 68°C) with Platinum Taq DNA High Fidelity
679 polymerase (Invitrogen) using 100 nM of genomic Alu forward primer 5′-
680 GCCTCCCAAAGTGCTGGGATTACAG and 600 nM of U3-reverse primer 5'-
681 CTTCTACCTTATCTGGCTCAAC-3'. The pre-amplification step was performed on serial dilutions
682 of all the DNA samples, as well as of a positive control (total DNA from U87-MG infected with a
683 high input of NL4-3), to ensure the linearity of the assay. Background levels were assessed using
684 linear, one-way amplification by performing the pre-amplification PCR with the U3-reverse primer
685 alone. Then a qPCR was performed on pre-amplification products using U3-forward primer 5'-
686 TCTACCACACACAAGGCTAC-3' and U3-reverse primer with the U3 probe 5'-[FAM]-
687 CAGAACTACACACCAGGGCCAGGGGTCA-[TAMRA]-3'. qPCR reactions were performed in
688 triplicates, in Universal PCR master mix using 900nM each primer and 250nM probe with the
689 following program: 10 min at 95°C followed by 40 cycles (15 sec at 95°C and 1 min at 60°C).
690 pNL4-3 or pTOPO-2LTR (generated by pTOPO cloning of a 2-LTR circle junction amplified from
691 NL4-3 infected cells, using oHC64 and U3-reverse primers into pCR™2.1-TOPO™) were diluted
692 in 20 ng/ml of salmon sperm DNA to create dilution standards used to quantify relative cDNA
693 copy numbers and confirm the linearity of all assays.
694
695 **Proximity Ligation assays (PLAs).** The proximity ligation assays were performed using the
696 Duolink® in situ Detection Reagents (Sigma-Aldrich, DUO92014). For PLA with HIV-1, MDMs
697 were plated in 24-well plates with coverslips pre-treated with poly-L-lysin (Sigma-Aldrich) and
698 infected with 1 μg $p24^{Gag}$ of HIV-1 NL4-3 (Ba-L Env) or mock-infected. For PLA with SARS-CoV-
699 2, A549-ACE2 cells were plated in 24-well plates with coverslips and infected at an MOI of 0,1.
700 24 h later, the cells were fixed with 2-4% paraformaldehyde in PBS1X for 10 min, washed in
701 PBS1X and permeabilized with 0.2% Triton X-100 for 10 min. After a couple of washes in PBS1X,
702 either NGB buffer (50 mM NH_4Cl, 2% goat serum and 2% bovine serum albumin in PBS) or
703 Duolink® blocking solution was added for 1h. Cells were incubated with mouse AG3.0 anti-HIV-

704 1 Capsid antibody (National Institutes of Health (NIH) AIDS Reagent Program #4121), or J2 anti-
705 dsRNA antibody (SCICONS), or anti-SARS-CoV-2 Nucleoprotein (N; BioVision), and rabbit anti-
706 DDX42 antibody (HPA023571, Sigma-Aldrich) diluted in NGB buffer or in Duolink® blocking
707 solution for 1h. After 2 washes in PBS1X, the cells were incubated with the DUOLINK® in situ
708 PLA® Probe Anti-rabbit minus (DUO92006) and DUOLINK® in situ PLA® Probe Anti-mouse plus
709 (DUO92001) for 1h at 37°C. After 2 washes in PBS1X, the ligation mix was added for 30 min at
710 37°C. After 2 washes in PBS1X, the cells were incubated with the amplification mix for 100 min
711 at 37°C followed by 3 washes in PBS1X. In the case of SARS-CoV-2 infection, an additional
712 staining was performed by incubating cells in an anti-mouse Alexa Fluor secondary antibody.
713 Finally, the cells were washed twice with PBS1X and stained with Hoechst at 1 μg/mL for 5 min,
714 washed again and the coverslips mounted on slides in Prolong mounting media (ThermoFisher
715 Scientific). Z-stack images were acquired using an LSM 880 confocal microscope (ZEISS) using
716 a 63x lens. PLA punctae quantification was performed using the FIJI software[66]. Briefly, maximum
717 z-projections were performed on each z-stack and the number of nuclei per field were quantified.
718 Then, by using a median filter and thresholding, PLA punctae were isolated and quantified
719 automatically using the Analyse Particles function. To obtain a mean number of dots per cell, the
720 number of PLA dots per field were averaged by the number of nuclei. In the case of SARS-CoV-
721 2 infection, the infected cells were identified using N or dsRNA immunofluorescence staining. For
722 representative images, single cells were imaged using a LSM880 confocal microscope coupled
723 with an Airyscan module. Processing of the raw Airyscan images was performed on the ZEN
724 Black software.
725
726 **Immunoblot analysis.** Cell pellets were lysed in sample buffer (200 mM Tris-HCl, pH 6.8, 5.2%
727 SDS, 20% glycerol, 0.1% bromophenol blue, 5% β-mercaptoethanol), resolved by SDS–PAGE
728 and analysed by immunoblotting using primary antibodies specific for human DDX42
729 (HPA023571, Sigma-Aldrich), Flag (M2, Sigma-Aldrich) and Actin (A1978, Sigma-Aldrich),
730 followed by secondary horseradish peroxidase-conjugated anti-mouse or anti-rabbit

731 immunoglobulin antibodies and chemiluminescence (Bio-Rad). Images were acquired on a
732 ChemiDoc™ gel imaging system (Bio-Rad).
733
734 **IAV production and infection.** We have described previously IAV NanoLuciferase reporter virus
735 generation[43]. Stocks were titrated by plaque assays on MDCK cells. IAV challenges were
736 performed in serum-free DMEM for 1 h and the medium was subsequently replaced with DMEM
737 containing 10%. IAV infection experiments were performed in triplicates in 96-well plates with
738 cultures maintained for 16 h post-challenge. NanoLuciferase activity was measured with the
739 Nano-Glo assay system (Promega), and luminescence was detected using a plate reader
740 (Infinite® 200 PRO, Tecan).
741
742 **VSV production and infection.** A VSV-G pseudotyped-VSV-Δenv reporter virus, coding both
743 GFP and Firefly Luciferase, was obtained from Gert Zimmer . The virus was amplified on pMD.G
744 transfected HEK293T and titrated thanks to the GFP reporter gene. For infection, 2.5 x 10^4 cells
745 per well in 96-well plates were infected at the indicated MOIs. 24h after infection, cells were lysed
746 and Firefly luciferase activity was measured (Firefly luciferase Assay System Promega).
747
748 **Measles virus production and infection.** Measles virus GFP strain (MeV-GFP), which was
749 kindly provided by F. Tangy (Institut Pasteur, Paris), was previously described[68]. Viral stocks were
750 produced on Vero NK cells. After 4 days of infection, supernatant was collected and then
751 centrifugated to eliminate dead cells or fragments. Stocks were tittered using median tissue
752 culture infectious dose assays ($TCID_{50}$) on Vero NK cells. Cells were infected with 10-fold serial
753 dilutions of viral stocks and incubated for 7 days. Cells were then washed with PSB and fixed with
754 3% formaldehyde crystal violet during 30 min and finally rinsed with water. For infections, Huh-7
755 cells were infected at the indicated multiplicity of infection (MOI) in DMEM without FBS for 2 h in
756 small volume of medium to enhance contacts with the inoculum and the cells. After 2 h, the viral
757 inoculum was replaced with fresh DMEM 10% FBS 1% P/S. 24 h post-infection the cells were
758 harvested and samples separated in half for Western blot and flow cytometry analysis.

759 **ZIKV production and infection.** The nanoluciferase expressing ZIKV construct has been
760 described[69]. The corresponding linearized plasmid was transcribed in vitro using the SP6
761 mMESSAGE mMACHINE™ (Thermofischer Scientific) and HEK293T cells were transfected with
762 the transcribed RNA. After 7 days, supernatants were harvested, filtered and stock titers were
763 determined by plaque assays on Vero cells. For infections, 2.5 x 10^4 cells per well in 96-well
764 plates were infected, at the indicated MOIs. 24h after infection, cells were lysed and
765 Nanoluciferase activity was measured using the Kit Nano Glo luciferase Assay (Promega).
766
767 **CHIKV production and infection.** The Nanoluciferase luciferase coding CHIKV construct was a
768 gift from Andres Merits. The linearized plasmid coding CHIKV genome was transcribed with the
769 T7 mMESSAGE mMACHINE kit (Thermofischer Scientific) and 5 x 10^5 HEK293T were
770 transfected with 1-4 μg of transcribed RNA, using Lipofectamine 2000 (Thermofischer Scientific).
771 After 24h, supernatants were harvested, filtered and viruses were then amplified on baby hamster
772 kidney (BHK21) cells. Stock titers were determined by plaque assays on Vero cells. For infections,
773 2.5 x 10^4 cells per well in 96-well plates were infected at the indicated MOIs. 24h after infection,
774 cells were lysed and Nanoluciferase activity was measured.
775
776 **SARS-CoV-2 production and infection.** The SARS-CoV-2 BetaCoV/France/IDF0372/2020
777 isolate was supplied by Pr. Sylvie van der Werf and the National Reference Centre for Respiratory
778 Viruses hosted by Institut Pasteur (Paris, France). The patient sample from which strain
779 BetaCoV/France/IDF0372/2020 was isolated was provided by Dr. X. Lescure and Pr. Y.
780 Yazdanpanah from the Bichat Hospital, Paris, France. The virus was amplified in Vero E6 cells
781 (MOI 0,005) in serum-free media supplemented with 0,1 μg/ml L-1-p-Tosylamino-2-phenylethyl
782 chloromethylketone (TPCK)-treated trypsin (Sigma-Aldrich). The supernatant was harvested at
783 72 h post infection when cytopathic effects were observed (with around 50% cell death), cell
784 debris were removed by centrifugation, and aliquots stored at -80C. Viral supernatants were
785 titrated by plaque assays in Vero E6 cells. Typical titers were 5.10^6 plaque forming units (PFU)/ml.
786 Infections of A549-ACE2 cells were performed at the indicated multiplicity of infection (MOI; as

787 calculated from titers obtained in Vero E6 cells) in serum-free DMEM and 5% serum-containing
788 DMEM, respectively. The viral input was left for the duration of the experiment and cells lysed at
789 48 h post-infection for RT-qPCR analysis.
790
791 **Statistical analyses.** Statistical analyses were performed with GraphPad Prism. Analysis types
792 are mentioned in Fig. legends and all comparisons are relative to the indicated controls. For data
793 with experimental factors greater than two, multiple linear regression was performed. For data
794 with two categorical factors, ANOVA was used, and repeated measures ANOVA when a pairing
795 factor was present. Simple linear regression was used when the relationship between a
796 continuous factor and a continuous response variable was investigated. P values are denoted as
797 follow: ns not significant, $p<0.05$ *, $p<0.01$ **, $p<0.001$ ***, $p<0.0001$****.
798
799
800 **Data availability**
801 The datasets generated during and/or analysed during the current study are available from the
802 corresponding authors on reasonable request.
803
804
805 **Requests for materials**
806 Requests for material should be addressed to Caroline Goujon at the corresponding address
807 above.
808
809
810 **Acknowledgements**
811 We wish to thank Tom Doyle and Chad Swanson for their useful comments on the manuscript,
812 and Matthieu Lewis, Nadine Laguette, Nathalie Arhel, Juliette Fernandez, Jean-Luc Battini, Georg
813 Kochs, Andres Merits, Frédéric Tangy, Sylvie van de Werf and Nathan Sherer for the generous

814 provision of reagents, protocols and/or for helpful discussions. We are grateful to Nicolas Manel
815 and Helena Izquierdo-Fernandez for sharing their protocol for efficient knockdown in primary
816 CD4+ T cell using CRISPR/Cas9 RNP electroporation. We are grateful to Myriam Boyer,
817 Stéphanie Viala, Baptiste Monterroso and Orestis Faklaris from the imaging and flow cytometry
818 facility MRI, for advice with flow cytometry and confocal microscopy, respectively. This work was
819 supported by the Institut National de la Santé et de la Recherche Médicale (INSERM) (to CG),
820 the ATIP-Avenir programme (to CG), institutional funds from the Centre National de la Recherche
821 Scientifique (CNRS) and Montpellier University, France REcherche Nord&Sud Sida/HIV et
822 Hépatites (ANRS) (ECTZ21792 to CG; ECTZ35478 to OM), Sidaction (to CG), a Starting Grant
823 from the European Research Council (759226, ANTIViR) (to CG), PhD studentships from the
824 Ministry of Higher Education and Research (to BB, JM and AR), and a 4th year PhD studentship
825 from the Fondation pour la Recherche Médicale (to BB). SR and HP acknowledge financial
826 support from the France Génomique National infrastructure, funded as part of "Investissement
827 d'Avenir" program managed by Agence Nationale de la Recherche (contract ANR-10-INBS-09).
828 We acknowledge the imaging facility MRI, member of the national infrastructure France-
829 BioImaging supported by the French National Research Agency (ANR-10-INBS-04) and the BSL-
830 3 facility CEMIPAI (UAR 3725 CNRS Montpellier University).
831
832
833 **Author contributions**
834 B.B. and CG designed the study, analysed the data and wrote the manuscript. B.B. and C.G.
835 performed the whole-genome screens and candidate validation. B.B. carried out most of the
836 experiments, with technical assistance from A.R., F.G.d.G, J.M., M.T., W.D., A.M., A.L.C.V.,
837 M.A.A., and O.M.; V.C. provided some of the lentiviral vector stocks; E.B. and L.B. performed
838 CHIKV infections, N.G. performed ZIKV-Nluc infections, S.G. and N.J. performed MeV, ZIKV
839 PF13, DENV-2 and YFV infections; M.L and E.R analysed the RNA-seq data; R.S. performed the
840 statistical analyses; H.P. and S.R. performed the Illumina sequencing and MaGECK analyses,
841 respectively. All authors have read and approved the manuscript.

842 **Conflicts of interest statement**

843 The authors have no conflicts of interest to declare in relation to this manuscript.

844 **References**

845 1. Schoggins, J. W. Interferon-Stimulated Genes: What Do They All Do? *Annu. Rev. Virol.* **6**, 567–584 (2019).

846 2. Lindenmann, J. Resistance of mouse to mice adapted influenza A virus. *Virology* **16**, 203–204 (1962).

847 3. Zhou, A. Expression cloning of 2-5A-dependent RNAase: A uniquely regulated mediator of interferon action.
848 *Cell* **72**, 753–765 (1993).

849 4. Zilberstein, A., Kimchi, A., Schmidt, A. & Revel, M. Isolation of two interferon-induced translational inhibitors:
850 a protein kinase and an oligo-isoadenylate synthetase. *Proc. Natl. Acad. Sci.* **75**, 4734–4738 (1978).

851 5. Kane, M. *et al.* Identification of Interferon-Stimulated Genes with Antiretroviral Activity. *Cell Host Microbe* **20**,
852 392–405 (2016).

853 6. OhAinle, M. *et al.* A virus-packageable CRISPR screen identifies host factors mediating interferon inhibition
854 of HIV. *eLife* **7**, e39823 (2018).

855 7. Schoggins, J. W. *et al.* A diverse range of gene products are effectors of the type I interferon antiviral
856 response. *Nature* **472**, 481–485 (2011).

857 8. Chemudupati, M. *et al.* From APOBEC to ZAP: Diverse mechanisms used by cellular restriction factors to
858 inhibit virus infections. *Biochim. Biophys. Acta Mol. Cell Res.* **1866**, 382–394 (2019).

859 9. Doyle, T., Goujon, C. & Malim, M. H. HIV-1 and interferons: who's interfering with whom? *Nat. Rev. Microbiol.*
860 **13**, 403–413 (2015).

861 10. Ghimire, D., Rai, M. & Gaur, R. Novel host restriction factors implicated in HIV-1 replication. *J. Gen. Virol.*
862 **99**, 435–446 (2018).

863 11. Goujon, C. *et al.* Human MX2 is an interferon-induced post-entry inhibitor of HIV-1 infection. *Nature* **502**,
864 559–562 (2013).

865 12. Kane, M. *et al.* MX2 is an interferon-induced inhibitor of HIV-1 infection. *Nature* **502**, 563–566 (2013).

866 13. Jimenez-Guardeño, J. M., Apolonia, L., Betancor, G. & Malim, M. H. Immunoproteasome activation enables
867 human TRIM5α restriction of HIV-1. *Nat. Microbiol.* (2019) doi:10.1038/s41564-019-0402-0.

868 14. Fan, W. *et al.* TRIM7 inhibits enterovirus replication and promotes emergence of a viral variant with
869 increased pathogenicity. *Cell* **184**, 3410-3425.e17 (2021).

870 15. Shalem, O. *et al.* Genome-scale CRISPR-Cas9 knockout screening in human cells. *Science* **343**, 84–87
871 (2014).

872 16. Shalem, O., Sanjana, N. E. & Zhang, F. High-throughput functional genomics using CRISPR-Cas9. *Nat.*
873 *Rev. Genet.* **16**, 299–311 (2015).

874 17. Sanjana, N. E., Shalem, O. & Zhang, F. Improved vectors and genome-wide libraries for CRISPR screening.
875 *Nat. Methods* **11**, 783–784 (2014).

876 18. Li, W. *et al.* MAGeCK enables robust identification of essential genes from genome-scale CRISPR/Cas9
877 knockout screens. *Genome Biol.* **15**, 554 (2014).
878 19. Doench, J. G. Am I ready for CRISPR? A user's guide to genetic screens. *Nat. Rev. Genet.* **19**, 67–80
879 (2018).
880 20. Goujon, C. *et al.* Evidence for IFNα-induced, SAMHD1-independent inhibitors of early HIV-1 infection.
881 *Retrovirology* **10**, 23 (2013).
882 21. Bulli, L. *et al.* Complex interplay between HIV-1 Capsid and MX2-independent IFNα-induced antiviral factors.
883 *J. Virol.* (2016) doi:10.1128/JVI.00458-16.
884 22. Xu, B., Pan, Q. & Liang, C. Role of MxB in Alpha Interferon-Mediated Inhibition of HIV-1 Infection. *J. Virol.*
885 **92**, (2018).
886 23. Uhlmann-Schiffler, H., Jalal, C. & Stahl, H. Ddx42p--a human DEAD box protein with RNA chaperone
887 activities. *Nucleic Acids Res.* **34**, 10–22 (2006).
888 24. Taschuk, F. & Cherry, S. DEAD-Box Helicases: Sensors, Regulators, and Effectors for Antiviral Defense.
889 *Viruses* **12**, (2020).
890 25. Granneman, S., Bernstein, K. A., Bleichert, F. & Baserga, S. J. Comprehensive Mutational Analysis of Yeast
891 DEXD/H Box RNA Helicases Required for Small Ribosomal Subunit Synthesis. *Mol. Cell. Biol.* **26**, 1183–
892 1194 (2006).
893 26. Rocak, S. Characterization of the ATPase and unwinding activities of the yeast DEAD-box protein Has1p
894 and the analysis of the roles of the conserved motifs. *Nucleic Acids Res.* **33**, 999–1009 (2005).
895 27. Ochsenbauer, C. *et al.* Generation of transmitted/founder HIV-1 infectious molecular clones and
896 characterization of their replication capacity in CD4 T lymphocytes and monocyte-derived macrophages. *J.*
897 *Virol.* **86**, 2715–2728 (2012).
898 28. Uhlmann-Schiffler, H., Kiermayer, S. & Stahl, H. The DEAD box protein Ddx42p modulates the function of
899 ASPP2, a stimulator of apoptosis. *Oncogene* **28**, 2065–2073 (2009).
900 29. Zyner, K. G. *et al.* Genetic interactions of G-quadruplexes in humans. *eLife* **8**, (2019).
901 30. Faulkner, G. J. & Billon, V. L1 retrotransposition in the soma: a field jumping ahead. *Mob. DNA* **9**, 22 (2018).
902 31. Liu, N. *et al.* Selective silencing of euchromatic L1s revealed by genome-wide screens for L1 regulators.
903 *Nature* **553**, 228–232 (2018).
904 32. Moran, J. V. *et al.* High frequency retrotransposition in cultured mammalian cells. *Cell* **87**, 917–927 (1996).
905 33. Wei, J. *et al.* Genome-wide CRISPR screens reveal host factors critical for SARS-CoV-2 infection. *Cell*
906 (2020) doi:10.1016/j.cell.2020.10.028.

907 34. Haller, O., Staeheli, P., Schwemmle, M. & Kochs, G. Mx GTPases: dynamin-like antiviral machines of innate
908 immunity. *Trends Microbiol.* **23**, 154–163 (2015).
909 35. Burdick, R. C. *et al.* HIV-1 uncoats in the nucleus near sites of integration. *Proc. Natl. Acad. Sci.* **117**, 5486–
910 5493 (2020).
911 36. Dharan, A., Bachmann, N., Talley, S., Zwikelmaier, V. & Campbell, E. M. Nuclear pore blockade reveals that
912 HIV-1 completes reverse transcription and uncoating in the nucleus. *Nat. Microbiol.* (2020)
913 doi:10.1038/s41564-020-0735-8.
914 37. Peng, K. *et al.* Quantitative microscopy of functional HIV post-entry complexes reveals association of
915 replication with the viral capsid. *eLife* **3**, e04114 (2014).
916 38. Zyner, K. G. *et al.* Genetic interactions of G-quadruplexes in humans. *eLife* **8**, e46793 (2019).
917 39. Fay, M. M., Lyons, S. M. & Ivanov, P. RNA G-Quadruplexes in Biology: Principles and Molecular
918 Mechanisms. *J. Mol. Biol.* **429**, 2127–2147 (2017).
919 40. Ruggiero, E. & Richter, S. N. G-quadruplexes and G-quadruplex ligands: targets and tools in antiviral
920 therapy. *Nucleic Acids Res.* **46**, 3270–3283 (2018).
921 41. Will, C. L. *et al.* Characterization of novel SF3b and 17S U2 snRNP proteins, including a human Prp5p
922 homologue and an SF3b DEAD-box protein. *EMBO J.* **21**, 4978–4988 (2002).
923 42. Goujon, C. *et al.* Characterization of Simian Immunodeficiency Virus SIVSM/Human Immunodeficiency Virus
924 Type 2 Vpx Function in Human Myeloid Cells. *J. Virol.* **82**, 12335–12345 (2008).
925 43. Doyle, T. *et al.* The interferon-inducible isoform of NCOA7 inhibits endosome-mediated viral entry. *Nat.*
926 *Microbiol.* **3**, 1369–1376 (2018).
927 44. Rebendenne, A. *et al.* SARS-CoV-2 triggers an MDA-5-dependent interferon response which is unable to
928 control replication in lung epithelial cells. *J. Virol.* (2021) doi:10.1128/JVI.02415-20.
929 45. Moncorge, O. *et al.* Investigation of Influenza Virus Polymerase Activity in Pig Cells. *J. Virol.* **87**, 384–394
930 (2013).
931 46. Adachi, A. *et al.* Production of acquired immunodeficiency syndrome-associated retrovirus in human and
932 nonhuman cells transfected with an infectious molecular clone. *J. Virol.* **59**, 284–291 (1986).
933 47. Simon, J. H., Southerling, T. E., Peterson, J. C., Meyer, B. E. & Malim, M. H. Complementation of vif-
934 defective human immunodeficiency virus type 1 by primate, but not nonprimate, lentivirus vif genes. *J. Virol.*
935 **69**, 4166–4172 (1995).
936 48. Schaller, T. *et al.* HIV-1 capsid-cyclophilin interactions determine nuclear import pathway, integration
937 targeting and replication efficiency. *PLoS Pathog.* **7**, e1002439 (2011).

938 49. Ryan-Graham, M. A. & Peden, K. W. C. Both Virus and Host Components Are Important for the Manifestation
939 of a Nef- Phenotype in HIV-1 and HIV-2. *Virology* **213**, 158–168 (1995).
940 50. Gaddis, N. C. *et al.* Further Investigation of Simian Immunodeficiency Virus Vif Function in Human Cells. *J.*
941 *Virol.* **78**, 12041–12046 (2004).
942 51. Naldini, L. *et al.* In vivo gene delivery and stable transduction of nondividing cells by a lentiviral vector.
943 *Science* **272**, 263–267 (1996).
944 52. Bainbridge, J. W. *et al.* In vivo gene transfer to the mouse eye using an HIV-based lentiviral vector; efficient
945 long-term transduction of corneal endothelium and retinal pigment epithelium. *Gene Ther.* **8**, 1665–1668
946 (2001).
947 53. O'Rourke, J. P., Newbound, G. C., Kohn, D. B., Olsen, J. C. & Bunnell, B. A. Comparison of gene transfer
948 efficiencies and gene expression levels achieved with equine infectious anemia virus- and human
949 immunodeficiency virus type 1-derived lentivirus vectors. *J. Virol.* **76**, 1510–1515 (2002).
950 54. Saenz, D. T., Teo, W., Olsen, J. C. & Poeschla, E. M. Restriction of feline immunodeficiency virus by Ref1,
951 Lv1, and primate TRIM5alpha proteins. *J. Virol.* **79**, 15175–15188 (2005).
952 55. Ostertag, E. M., Prak, E. T., DeBerardinis, R. J., Moran, J. V. & Kazazian, H. H. Determination of L1
953 retrotransposition kinetics in cultured cells. *Nucleic Acids Res.* **28**, 1418–1423 (2000).
954 56. Goodier, J. L., Cheung, L. E. & Kazazian, H. H. MOV10 RNA Helicase Is a Potent Inhibitor of
955 Retrotransposition in Cells. *PLoS Genet.* **8**, e1002941 (2012).
956 57. Nakabayashi, H., Taketa, K., Miyano, K., Yamane, T. & Sato, J. Growth of human hepatoma cells lines with
957 differentiated functions in chemically defined medium. *Cancer Res.* **42**, 3858–3863 (1982).
958 58. Wingett, S. W. & Andrews, S. FastQ Screen: A tool for multi-genome mapping and quality control.
959 *F1000Research* **7**, 1338 (2018).
960 59. Martin, M. Cutadapt removes adapter sequences from high-throughput sequencing reads. *EMBnet.journal*
961 **17**, 10–12 (2011).
962 60. Langmead, B., Trapnell, C., Pop, M. & Salzberg, S. L. Ultrafast and memory-efficient alignment of short DNA
963 sequences to the human genome. *Genome Biol.* **10**, R25 (2009).
964 61. Li, H. *et al.* The Sequence Alignment/Map format and SAMtools. *Bioinforma. Oxf. Engl.* **25**, 2078–2079
965 (2009).
966 62. Goujon, C. & Malim, M. H. Characterization of the alpha interferon-induced postentry block to HIV-1 infection
967 in primary human macrophages and T cells. *J. Virol.* **84**, 9254–9266 (2010).
968 63. Corman, V. M. *et al.* Detection of 2019 novel coronavirus (2019-nCoV) by real-time RT-PCR. *Euro Surveill.*
969 *Bull. Eur. Sur Mal. Transm. Eur. Commun. Dis. Bull.* **25**, (2020).

970 64. Meertens, L. *et al.* FHL1 is a major host factor for chikungunya virus infection. *Nature* **574**, 259–263 (2019).
971 65. Zürcher, T., de la Luna, S., Sanz-Ezquerro, J. J., Nieto, A. & Ortín, J. Mutational analysis of the influenza
972 virus A/Victoria/3/75 PA protein: studies of interaction with PB1 protein and identification of a dominant
973 negative mutant. *J. Gen. Virol.* **77 (Pt 8)**, 1745–1749 (1996).
974 66. Schindelin, J. *et al.* Fiji: an open-source platform for biological-image analysis. *Nat. Methods* **9**, 676–682
975 (2012).
976 67. Rentsch, M. B. & Zimmer, G. A Vesicular Stomatitis Virus Replicon-Based Bioassay for the Rapid and
977 Sensitive Determination of Multi-Species Type I Interferon. *PLoS ONE* **6**, (2011).
978 68. Combredet, C. *et al.* A molecularly cloned Schwarz strain of measles virus vaccine induces strong immune
979 responses in macaques and transgenic mice. *J. Virol.* **77**, 11546–11554 (2003).
980 69. Mutso, M. *et al.* Reverse genetic system, genetically stable reporter viruses and packaged subgenomic
981 replicon based on a Brazilian Zika virus isolate. *J. Gen. Virol.* **98**, 2712–2724 (2017).
982

983 **SUPPLEMENTARY INFORMATION**

984

985 **Supplemental methods**

986 Only the methods specific for the supplemental Figures are described here.

987

988 **Plasmids**. pBlaM-Vpr and pAdVAntage have been described[70].

989

990 **Lentiviral production**. β-lactamase-Vpr (BlaM-Vpr)-carrying viruses, bearing the wild-type Env,
991 were produced by co-transfection of HEK293T cells with the NL4-3/Nef-IRES-Renilla provirus
992 expression vector, pBlaM-Vpr and pAdVAntage at a ratio of 4:1:0.5, as previously described[70].
993 Viral particles were titrated using an HIV-1 $p24^{Gag}$ Alpha-Lisa kit and an Envision plate reader
994 (Perkin Elmer).

995

996 **BlaM-Vpr assay for HIV-1 entry.** This assay was performed as described previously[62]. Briefly, 2
997 x 10^5 U87-MG/CD4/CXCR4 cells were plated in 24-well plates and incubated with BlaM-Vpr
998 carrying NL4-3 particles (31, 62, 125 ng $p24^{Gag}$) or mock-infected for 3 h at 37°C. The cells were
999 then washed once in CO_2-independent medium and loaded with CCF2-AM substrate-containing
1000 solution (ThermoFisher Scientific) for 1 h at room temperature before 2 washes and incubation at
1001 room temperature for 16 h in development medium (CO_2-independent medium containing 2,5 mM
1002 probenecid). Finally, the cells were trypsinized, washed and fixed in 1% paraformaldehyde (PFA)-
1003 PBS1X before analysis with a FACSCanto™ II (Becton Dickinson).

1004

1005 **Viruses and infection.** The Yellow Fever Virus (YFV) Asibi strain was provided by the Biological
1006 resource Center of Institut Pasteur. Stocks were produced on Vero NK cells. After 3 days of
1007 infection, viruses were concentrated by polyethylene glycol 6000 (PEG) precipitation and purified
1008 by centrifugation in a discontinuous gradient of sucrose. The Dengue 2 strain Malaysia SB8553
1009 (DENV-2) was obtained from the Centro de Ingeniería Genética y Biotecnología (CIGB), Cuba.
1010 Stocks were generated on Vero NK cells. After 4 days of infection, viruses were concentrated by

1011 PEG 6000 precipitation. The Zika strain PF13 (kindly provided by V. M. Cao-Lormeau and D.
1012 Musso, Institut Louis Malardé, Tahiti Island, French Polynesia) was isolated from a viremic patient
1013 in French Polynesia in 2013. Stocks were produced on C6-36 cells. After 2 days of infection,
1014 viruses were concentrated by PEG 6000 precipitation and purified by centrifugation in a
1015 discontinuous gradient of sucrose. YFV Asibi and ZIKV titers were assessed by plaque assays
1016 using Vero NK cells, as described previously[71]. DENV-2 was tittered by in cell western assays on
1017 Vero cells. Cells were fixed with PFA 4% during 30 min at room temperature (RT), then washed
1018 in PBS and permeabilized with 0,5% triton in PBS (Sigma-Aldrich) during 10 min at RT. Cells
1019 were then incubated 0,1% Tween in PBS (Sigma-Aldrich) containing 5% BSA (Sigma-Aldrich)
1020 during 1 h at RT prior to incubation with mouse anti-Env 4G2 antibodies overnight at 4°C. After
1021 1h of incubation with the secondary antibodies, cells were revealed with an Odyssey CLx infrared
1022 imaging system (Li-Cor Bioscience).
1023 Cells were infected at the indicated multiplicity of infection (MOI) in DMEM without FBS for 2 h in
1024 small volume of medium to enhance contacts with the inoculum and the cells. After 2 h, the viral
1025 inoculum was replaced with fresh DMEM 10% FBS 1% P/S. 24 hours post-infection the cells were
1026 harvested and samples separated in half for Western blot and flow cytometry analysis. For the
1027 latter, cells were fixed and permeabilized using BD Cytofix/Cytoperm (Fisher scientific) for 30 min
1028 on ice (all the following steps were performed on ice and centrifuged at 4°C) and then washed
1029 tree times with wash buffer. Cells infected with YFV, ZIKV and DENV-2 were incubated with the
1030 pan-flavivirus anti-Env 4G2 antibody for 1 h at 4°C and then with Alexa 488 anti-mouse IgG
1031 secondary antibodies (Thermo Fisher) for 45 min at 4°C in the dark. Data were acquired with an
1032 Attune NxT Acoustic Focusing Cytometer (Life technologies) and analyzed using FlowJo
1033 software.
1034
1035 **Quantification of mRNA expression**. For all Figures except Fig. S4, see the main material and
1036 methods; For Fig. S4: a TaqMan gene expression assays (Applied Biosystem) specific for ISG15
1037 was used: Hs00192713_m1.

1038 For the RNA extraction and RT-qPCR analysis specifically in Huh-7 cells, total RNAs were
1039 extracted from cell lysates using the NucleoSpin RNA II kit (Macherey-Nagel), following the
1040 manufacturer's protocol. Equal amounts of purified total RNA were used to synthetized first strand
1041 cDNA using random hexamers (Thermo Fisher) and the ReverAid H Minus Moloney murine
1042 leukemia virus (M-MuLV) reverse transcriptase (Thermo Fisher). Quantitative real-time PCR was
1043 performed on a real-time PCR system (Quant Studio 6 Flex from Applied Biosytems) with SYBR
1044 green PCR master mix (Life Technologies). Data were analyzed with the ΔΔ CT method. All the
1045 samples were performed in technical triplicate and normalized to GAPDH (glyceraldehyde-3-
1046 phosphate dehydrogenase) as endogenous reference control. The primer sequences used for
1047 Fig. S4 were as follow: GAPDH Forward: 5'-GGTCGGAGTCAACGGATTTG-3', reverse: 5'-
1048 ACTCCACGACGTACTCAGCG-3'; DDX42 Forward: 5'-GGCCTATACCCTACTCACTCCC-3',
1049 reverse: 5'-CCACCAATGTTCAGCTTTTTTCC-3'.
1050
1051 **Preparation of RNA-seq libraries.** siRNA transfected U87-MG/CD4/CXCR4 and A549-ACE2
1052 RNA extracts from three independent experiments were used for RNA-seq library preparation.
1053 After determining sample RNA integrity numbers using a 2100 Bioanalyzer (Agilent), ribosomal
1054 RNAs were depleted using the QIAseq FastSelect -rRNA HMR Kit (Qiagen) and libraries were
1055 prepared according to manufacturer's instructions using the QIAseq Stranded Total RNA Lib Kit
1056 (Qiagen). Libraries were quantified using a TapeStation D1000 ScreenTape. Equimolar amounts
1057 of each library were then mixed and sequenced on 2 lanes (2x150 bp) on the Illumina HiSeq
1058 3000/4000 platform (GENEWIZ).
1059
1060 **Analysis of high-throughput sequencing reads.** Sequenced reads were filtered by quality and
1061 sequence adaptors removed using fastp v0.20.1 (https://github.com/OpenGene/fastp)[72] with
1062 following parameters "fastp --qualified_quality_phred 20 --disable_length_filtering --
1063 detect_adapter_for_pe". Reads were pseudo-mapped against human cDNA sequenced
1064 downloaded from Gencode database (https://www.gencodegenes.org/) and transcripts

1065 abundance estimated with Kallisto v0.46.2 (https://pachterlab.github.io/kallisto/about)[73] with
1066 parameters "--bias --bootstrap-samples 100".
1067
1068 **Differential analysis with DESeq2.** Differential expressed genes upon siRNA transfection were
1069 obtained using DESeq2[74] (version 1.32.0) in R (version 4.1.0). Briefly, transcript estimations were
1070 transformed in gene counts with tximport package[75] and the differential expression obtained with
1071 the model design "~ condition + replicate".
1072
1073 **Supplementary Information References**
1074
1075 70. Cavrois, M., de Noronha, C. & Greene, W. C. A sensitive and specific enzyme-based assay detecting
1076 HIV-1 virion fusion in primary T lymphocytes. *Nat. Biotechnol.* **20**, 1151–1154 (2002).
1077 71. Beauclair, G. *et al.* Retinoic Acid Inducible Gene I and Protein Kinase R, but Not Stress Granules,
1078 Mediate the Proinflammatory Response to Yellow Fever Virus. *J. Virol.* **94**, (2020).
1079 72. Chen, S., Zhou, Y., Chen, Y. & Gu, J. fastp: an ultra-fast all-in-one FASTQ preprocessor. *Bioinformatics*
1080 **34**, i884–i890 (2018).
1081 73. Bray, N. L., Pimentel, H., Melsted, P. & Pachter, L. Near-optimal probabilistic RNA-seq quantification.
1082 *Nat. Biotechnol.* **34**, 525–527 (2016).
1083 74. Love, M. I., Huber, W. & Anders, S. Moderated estimation of fold change and dispersion for RNA-seq
1084 data with DESeq2. *Genome Biol.* **15**, 550 (2014).
1085 75. Soneson, C., Love, M. I. & Robinson, M. D. Differential analyses for RNA-seq: transcript-level estimates
1086 improve gene-level inferences. *F1000Research* **4**, 1521 (2015).
1087

1088 **Supplementary Figures**

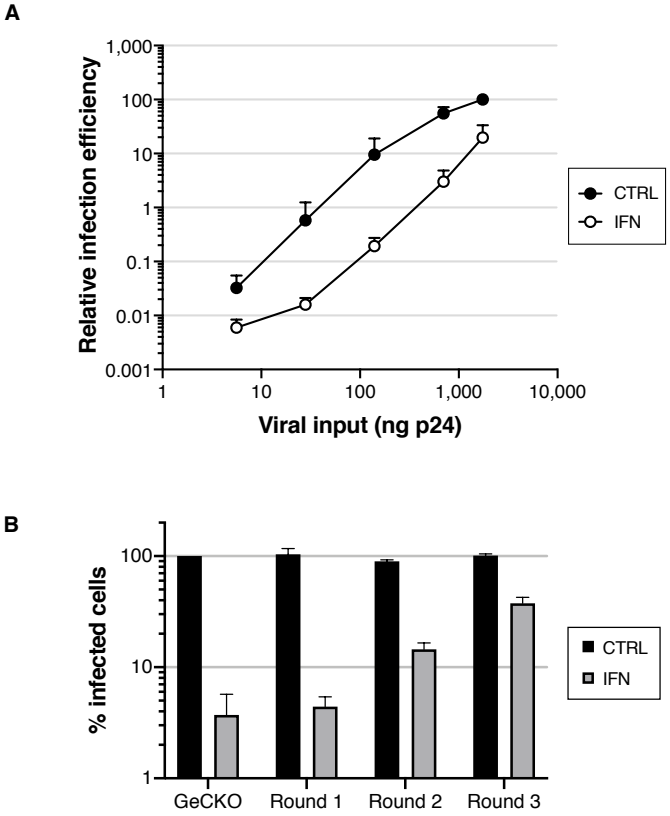

1089

1090 **Figure S1. Related to Figure 1.**

1091 **A. IFN pre-treatment potently inhibits HIV-1 infection in T98G cells and is, at least partially, saturable.**
1092 T98G/Cas9/CD4/CXCR4/ Firefly cells were pre-treated with IFN for 24 h prior to infection with increasing doses
1093 of NL4-3 Renilla (indicated in ng $p24^{Gag}$). Renilla activity was normalized to Firefly activity and the relative
1094 infection efficiencies are shown. Data represent the average of 3 independent experiments and one standard
1095 deviation from the mean.

1096 **B. GeCKO screen validation.** GeCKO control cells and enriched cells from 3 successive rounds of selection
1097 (Round 1, 2, and 3, as indicated) were treated with IFN or not and infected with GFP-expressing lentiviral vectors.
1098 The percentage of infected cells was evaluated by flow cytometry 2 days post-infection. Data represent the
1099 average of 2 independent experiments and one standard deviation from the mean.

1100

1101

1102

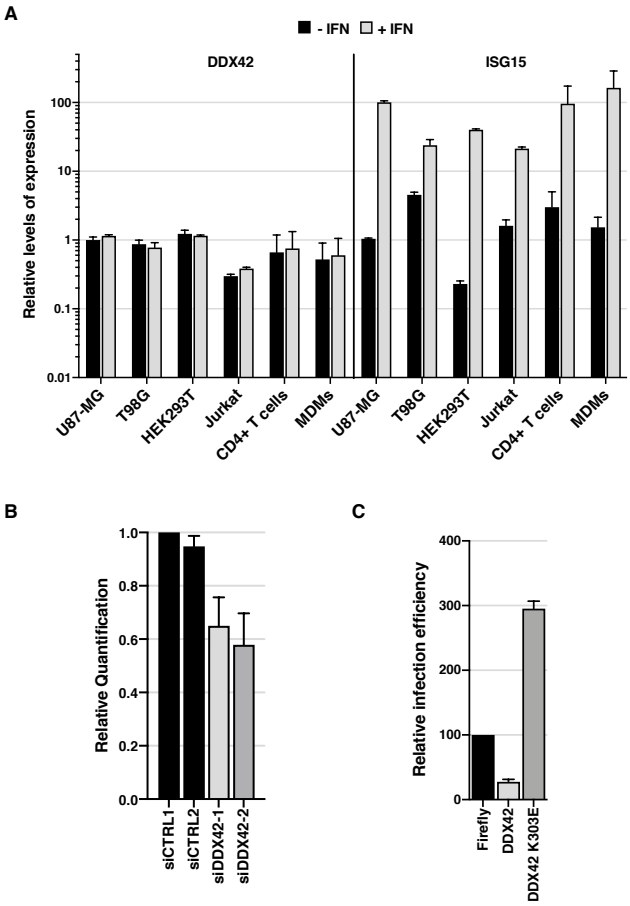

Figure S2. Related to Figure 2.

A. DDX42 is not an ISG. The indicated primary cells or immortalized cell cultures were treated with IFN for 24 h or left untreated. RNA was subsequently extracted and DDX42 and ISG15 (a prototype ISG) mRNA levels were quantified by RT-qPCR; Actin B and GAPDH were used as endogenous controls. The bar chart shows the relative levels of expression of DDX42 and ISG15 in the presence or absence of IFN treatment. Data represent the mean ± S.E.M of 3 independent experiments.

B. DDX42 silencing efficiency in monocyte-derived macrophages. siRNA-transfected MDMs were harvested 48h post-transfection for RNA extraction and quantification of DDX42 mRNA levels by RT-qPCR. Actin and GAPDH were used as endogenous controls. Data represent the mean ± S.E.M of 3 independent experiments performed with cells from 3 different blood donors (parallel samples from Fig. 2E).

C. Ectopic expression of DDX42 K303E mutant increases HIV-1 infection. U87-MG/CD4/CXCR4 cells were transduced with lentiviral vectors expressing either Firefly (negative control), WT DDX42 (DDX42) or a motif I mutant DDX42 K303, which has an impaired ATPase activity (DDX42 K303E). Transduced cells were infected with NL4-3 Renilla and the infection efficiency was assessed 24h later by measuring Renilla activity. Data represent the mean ± S.E.M of 4 independent experiments.

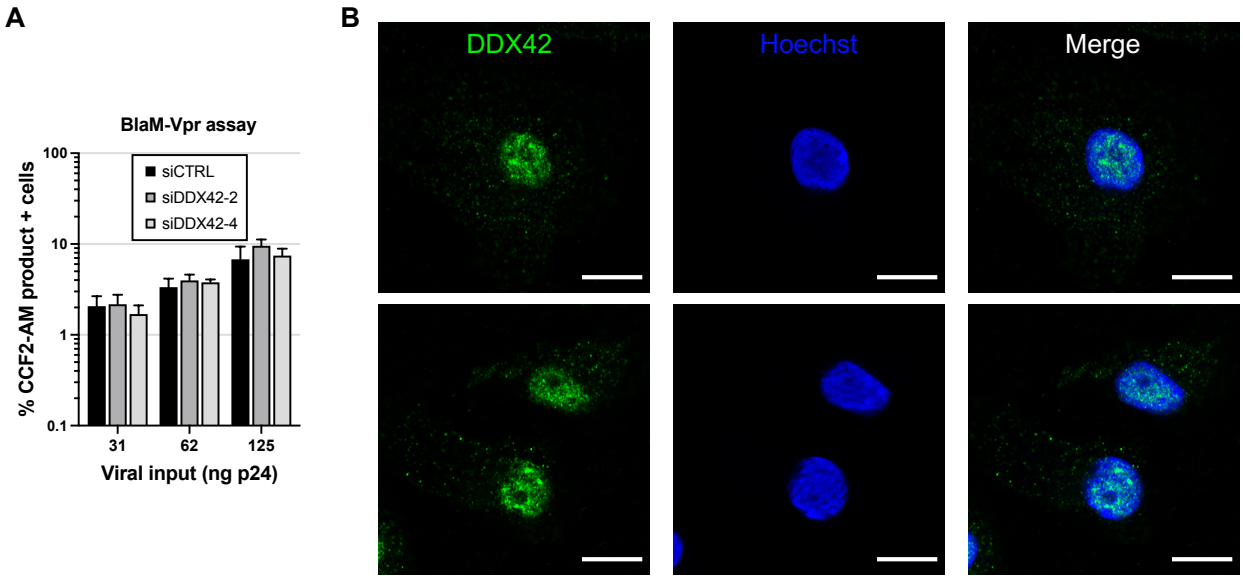

1121

1122 **Figure S3. Related to Figure 3.**

1123 **A. DDX42 depletion does not affect HIV-1 entry.** DDX42-depleted U87-MG/CD4/CXCR4 cells were infected
1124 with the indicated amounts of viruses carrying the β-lactamase (BlaM)-Vpr fusion protein for 3 h. The cells were
1125 subsequently loaded with CCF2-AM substrate dye for 2h, washed extensively and incubated for another 16 h for
1126 the reaction to develop. Cells positive for the CCF2-AM product were scored by flow cytometry. Data represent
1127 the mean ± S.E.M of 3 independent experiments.

1128 **B. DDX42 localization in MDMs.** MDMs were fixed, endogenous DDX42 and the nuclei were visualized using
1129 DDX42-specific antibodies and Hoechst staining, respectively, and confocal microscopy. Representative images
1130 are shown. Scale bar, 10 μm.

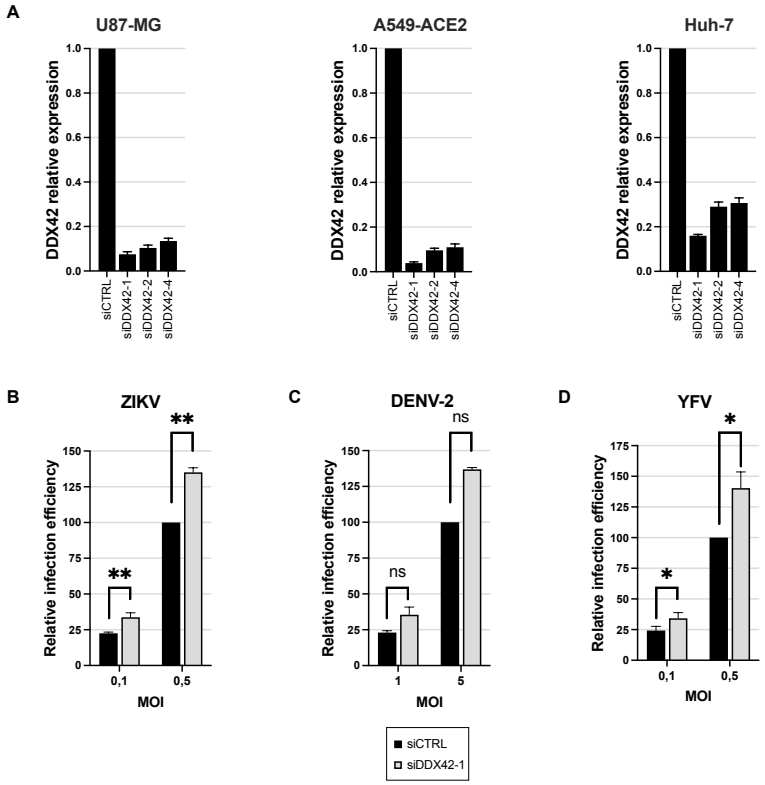

Figure S4. Related to Figure 4.

A. DDX42 silencing efficiency in U87-MG, A549-ACE2 and Huh-7 cells.

B. Relative ZIKV PF13 infection efficiency in siRNA-transfected Huh-7 cells analysed by flow cytometry.

C. Relative DENV-2 infection efficiency in siRNA-transfected Huh-7 cells analysed by flow cytometry.

D. Relative YFV infection efficiency in siRNA-transfected Huh-7 cells analysed by flow cytometry.

A-D. Mean ± SEM of 3 independent experiments (4 for silencing efficiency in A549-ACE2 cells). Two-way ANOVA with Sidak's test on log10 transformed data.

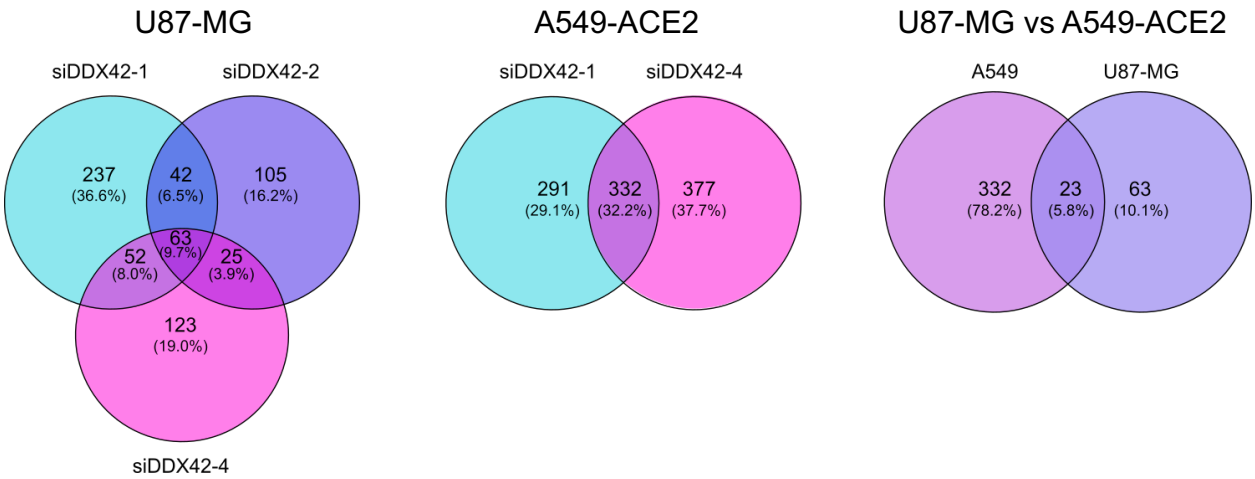

Figure S5.

Venn diagrams showing the Differentially Expressed Genes (DEGs) overlap between siRNA conditions in U87-MG cells, A549 cells and DEGs overlapping between U87-MG and A549 cells using cutoff criteria of log2 fold change (log2FC) >1 and p value <0.05.

See **Supplemental File 1** for the identity of the DEGs.